Biomedicine & Pharmacotherapy 150 (2022) 112994

Contents lists available at ScienceDirect

Biomedicine & Pharmacotherapy

journal homepage: www.elsevier.com/locate/biopha

Dietary administration of D-chiro-inositol attenuates sex-specific metabolic imbalances in the 5xFAD mouse model of Alzheimer's disease

Antonio J. López-Gambero [a,b,c], Beatriz Pacheco-Sánchez [a], Cristina Rosell-Valle [a], Dina Medina-Vera [a,c,d,e], Juan Antonio Navarro [a,b,d], María del Mar Fernández-Arjona [a,b], Marialuisa de Ceglia [a,b], Carlos Sanjuan [f], Vincent Simon [g], Daniela Cota [g], Patricia Rivera [a,b], Fernando Rodríguez de Fonseca [a,b,*], Juan Suárez [a,d,h,**]

[a] Instituto de investigación Biomédica de Málaga-IBIMA, 29010 Málaga, Spain
[b] UGC Salud Mental, Hospital Regional Universitario de Málaga, 29010 Málaga, Spain
[c] Universidad de Málaga, Andalucia Tech, Departamento de Biología Celular, Genética y Fisiología, Campus de Teatinos s/n, 29071 Málaga, Spain
[d] Universidad de Málaga, Andalucia Tech, Facultad de Medicina, Campus de Teatinos s/n, 29071 Málaga, Spain
[e] UGC Corazón, Hospital Universitario Virgen de la Victoria, 29010 Málaga, Spain
[f] EURONUTRA S.L, Parque Tecnológico de Andalucía, Campanillas, 29590, Spain
[g] University of Bordeaux, INSERM, Neurocentre Magendie, U1215, 33000 Bordeaux, France
[h] Departamento de Anatomía Humana, Medicina Legal e Historia de la Ciencia, Universidad de Málaga, 29071 Málaga, Spain

ARTICLE INFO

Keywords:
Alzheimer's disease
D-chiro-inositol
Hypothalamus
Inflammation
Insulin signaling
Fatty liver disease

ABSTRACT

Increasing evidence shows that hypothalamic dysfunction, insulin resistance, and weight loss precede and progress along with the cognitive decline in sporadic Alzheimer's Disease (AD) with sex differences. This study aimed to determine the effect of oral dietary administration of D-Chiro-inositol (DCI), an inositol used against insulin resistance associated with polycystic ovary, on the occurrence of metabolic disorders in the transgenic 5xFAD mouse model of AD (FAD: Family Alzheimer's Disease). DCI was administered from 6 to 10 months of age to male and female 5xFAD mice and control (non-Tg) littermates. Energy balance and multiple metabolic and inflammatory parameters in the hypothalamus, liver and plasma were evaluated to assess the central and peripheral effects of DCI. Results indicated that weight loss and reduced food intake in 5xFAD mice were associated with decreased neuropeptides controlling food intake and the appearance of a pro-inflammatory state in the hypothalamus. Oral administration of DCI partially restored energy balance and hypothalamic parameters, highlighting an increased expression of *Npy* and *Agrp* and female-specific downregulation of *Gfap* and *Igf1*. DCI also partially normalized impaired insulin signaling and circulating insulin, GLP-1, and GIP deficiencies in 5xFAD mice. Principal component analysis of metabolic parameters indicated the presence of a female-specific fatty liver in 5xFAD mice: DCI administration reversed hepatic fat accumulation, β-oxidation, inflammation and increased GOT and GPT levels. Our study depicts that metabolic impairment along with the cognitive decline in a mouse model of AD, which is exacerbated in females, can be ameliorated by oral supplementation with insulin-sensitizing DCI.

1. Introduction

As life expectancy increases, so does the public health and socioeconomic impact of age-related degenerative disorders that lead to cognitive decline and severe disability. Alzheimer's disease (AD) is a major age-related neurodegenerative disorder, mostly sporadic in

* Correspondence to: Instituto de investigación Biomédica de Málaga-IBIMA, Avenida Carlos Haya 82, 29010 Málaga, Spain.
** Correspondence to: Departamento de Anatomía Humana, Medicina Legal e Historia de la Ciencia, Facultad de Medicina, Universidad de Málaga, Bulevar Louis Pausteur 32, 29071 Málaga, Spain.
E-mail addresses: antonio.lopez@ibima.eu (A.J. López-Gambero), beatriz.pacheco@ibima.eu (B. Pacheco-Sánchez), cristina.rosell@ibima.eu (C. Rosell-Valle), dina.medina@ibima.eu (D. Medina-Vera), juan_naga@hotmail.es (J.A. Navarro), marfernandez@uma.es (M.M. Fernández-Arjona), marialuisa.deceglia@ibima.eu (M. de Ceglia), euronutra@euronutra.eu (C. Sanjuan), vincent.simon@inserm.fr (V. Simon), daniela.cota@inserm.fr (D. Cota), patricia.rivera@ibima.eu (P. Rivera), fernando.rodriguez@ibima.eu (F. Rodríguez de Fonseca), juan.suarez@uma.es (J. Suárez).

https://doi.org/10.1016/j.biopha.2022.112994
Received 25 February 2022; Received in revised form 13 April 2022; Accepted 17 April 2022
Available online 26 April 2022

origin, and the leading cause of dementia in 60–80% of cases [1]. AD is characterized by the loss of cognitive functions such as memory, reasoning or language, and leads to death approximately 3–9 years after diagnosis. Common features of AD are the aggregation and deposition of amyloid-β (Aβ) in plaques, and the deposition of the Tau protein, secondary to its hyperphosphorylation, leading to the formation of neurofibrillary tangles [2,3]. These events are associated with neuroinflammation and irreversible neuronal damage.

Although unhealthy dietary habits, obesity, and cardiovascular problems are well-established risk factors for the onset of AD, an opposing trend shows that weight loss and low body mass index (BMI) are associated with the progression of neurodegenerative diseases such as AD in the elderly [4]. Patient follow-up studies have found that the onset of dementia in AD is preceded by weight loss earlier in life and BMI is also negatively correlated with the presence of AD markers (Aβ and total Tau) in cerebrospinal fluid (CSF) and misfolded Aβ in plasma even in normal individuals [5–7]. In contrast, overweight individuals are less likely to show elevated levels of AD biomarkers, suggesting that AD develops from heterogeneous pathophysiology in this population [6,7]. These studies, however, are based on non-familial AD, since less than 5% of cases are related to familial AD.

Hypothalamic dysfunction also contributes to AD development in the early stages. Magnetic resonance imaging (MRI) and electron microscopy (EM) studies have demonstrated the presence of hypothalamic atrophy, decreased neuronal population and neuronal dystrophy in the hypothalamus of early AD patients [8,9]. Although the inflammatory response is strongly present in the hypothalamus, Aβ deposition is not associated with hypothalamic dysfunction [8,10]. A loss of function of NPY/AgRP producing orexigenic neurons has been detailed in animal models of AD, resulting in a decreased pattern of food intake [10–12]. Hypothalamic neurons also become less responsive to hormones that control energy status such as insulin, leptin, or ghrelin, leading to defective regulation of energy balance [10,13].

Metabolic disturbances in the peripheral organs also seem to correlate with and contribute to the onset of AD. Follow-up studies have shown that low fasting plasma insulin levels were predictors of increased risk of dementia and AD, compared with high insulin levels, and this association was independent of preclinical type 2 diabetes mellitus (T2DM) [14,15]. The low insulin levels observed in 5xFAD, 3xTg, and Tg2576 mouse models of AD support a role of insulin in AD pathology [10,16,17]. Alterations in other circulating factors such as leptin, ghrelin, or gonadotropins have also been associated with AD [18–20]. However, there are still few studies that combine the plasma levels of these factors as a predictive model of AD.

Given the importance of the liver as a key reservoir of energy and its detoxification activity, several studies have reported that increased ratio of the liver enzymes aspartate aminotransferase (AST/GOT) and alanine aminotransferase (ALT/GPT) are associated with the diagnosis of AD, impaired cognitive performance, increased deposition of Aβ and hyperphosphorylated tau in CSF, along with low brain metabolic activity [21]. Inflammatory and impaired metabolism in the liver can lead to low hepatic clearance of circulating Aβ, exacerbating AD pathology [22,23].

Inositols are important components in insulin signaling. One of the most important inositol isomers is D-chiro inositol (DCI; cis-1,2,4-trans-3,5,6-cyclohexanehexol). Although Myo-inositol is converted to DCI in the organism via an epimerase, the diet provides the greatest amount of DCI to the body, as it is found in large amounts in its 3-O-methylated form (D-Pinitol) in certain plant products, including carob pods and legumes [24]. DCI is present in cell membranes in the form of DCI-phosphoglycans (DCI-IPGs), and acts as a secondary messenger in insulin signaling pathways upon insulin receptor-mediated cleavage and release by specific phospholipases [2]. DCI combined with the disaccharide galactosamine is an allosteric modulator of the α isoform of protein phosphatase 2 C (PP2Cα) [25] and mitochondrial PDH phosphatase (PDHP) [26], through which they promote glucose internalization, glycogen synthesis, and modulation of lipid metabolism. D-Pinitol and DCI-IPG promote insulin release in a similar and synergistic mechanism to that of glucose [27–29]. However, DCI administration reduces insulin levels in hyperinsulinemia by acting directly on target tissues as a second messenger, thus reducing the increased insulin requirements [30]. DCI administration also promotes adipocyte lipogenesis and improves hepatic metabolism, thus exerting a hepatoprotective role [31–33].

Although inositols such as DCI could be a potential treatment to preserve insulin deficiency signaling in the brain (3,39,49), few studies are available regarding the insulin resistance observed in AD patients and the use of therapeutic agents targeting AD-associated metabolic disorders outside the framework of diabetes mellitus. In the present study, we explored the effect of DCI in an animal model of AD, the 5xFAD mouse, which carries 5 human mutations that lead to overexpression of APP and PS1 proteins, resulting in early Aβ deposition and an inflammatory response observed by histology in cortex and hippocampus, among other brain areas [34–36]. Aβ accumulation can be observed as early as 2 months of age in the cortex, and also in the hippocampus at 6 months of age along with astrogliosis and microgliosis [34–36]. Cognitive impairment can be observed at approximately 5–6 months of age, as seen in impaired spontaneous alternation in Y-Maze and also in impaired spatial memory displayed in the Morris Water Maze (MWM) test [34–36]. 5xFAD mice also reproduce a metabolic pathology of AD at an early age, including hypoinsulinemia and negative energy balance [10,37]. Therefore, we chose this animal model of AD to study the effect of DCI on changes in metabolism that occur between 6 and 10 months of age, in the onset of cognitive symptoms. We focused on the hypothalamus, the endocrine system, and the metabolic profile of the liver. Given the beneficial effect of DCI on both, gonadotrophin and sex-steroid hormones secretion (the reason for use of DCI in polycystic ovary syndrome) and the higher incidence of AD in women, we also studied whether DCI treatment produced a sex-specific effect.

2. Materials and methods

2.1. Ethics statement

The research procedures were approved by the Research and Clinical Ethics Committee of the Regional University Hospital of Malaga and the University of Malaga. All experimental procedures with animals comply with the ARRIVE guidelines and were carried out in strict accordance with the EU Directive 2010/63/EU for animal experiments. Every effort was made to minimize animal suffering, as well as to reduce the number of animals used.

2.2. Animals

The animals used were non-transgenic (non-Tg) and homozygous (5xFAD) male and female mice of 6 months of age (non-Tg males n = 8, DCI treated non-Tg males n = 9, 5xFAD males n = 7, DCI-treated 5xFAD males n = 8, non-Tg females n = 7, DCI-treated non-Tg females n = 6, 5xFAD females n = 8, DCI-treated 5xFAD females n = 7). 5xFAD mice co-express and co-inherit familial Alzheimer's disease (FAD) mutant forms of human transgenes for APP (the Swedish mutation: K670N, M671L; the Florida mutation: 1716 V; the London mutation: V7171) and PSI (M146L; L286V) under transcriptional control of the neuron-specific mouse Thy-1 promotor (Tg6799 line) [34]. 5xFAD lines (B6/SJL genetic background) were maintained by crossing heterozygous transgenic mice with B6/SJL F1 breeders (The Jackson Laboratory, Bar Harbor, ME, USA). Wild-type non-Tg littermate mice served as control, given the absence of Aβ deposition in the brain at 6 months of age (a hallmark of 5xFAD mice) and lack of cognitive impairment and metabolic imbalances [35–37].

The rodents were housed in the Animal Center for Experimentation at the University of Malaga with free access to food and water under

standardized conditions: 20 ± 2 °C of room temperature, relative humidity of 40 ± 5%, and a light/dark cycle of 12 h with dawn/sunset effect. This Center complies with all current regulations for breeding and housing. Animals were housed individually when experimental procedures required the control of dietary supplementation of DCI and the accurate measurement of food consumption. Mice were fed with a standard pellet diet (STD) (3.02 Kcal/g with 30 Kcal% protein, 55 Kcal% carbohydrates, and 15 Kcal% fat; purchased from Harlam (Tecklad, Madison WI, USA)). The diet was supplemented with DCI (Caromax DCI, 98% purity, provided by EURONUTRA SL, Málaga, SPAIN) ad libitum in their drinking water for 4 months from 6 months of age. Daily doses were 200 mg/kg/day, as a dissolved powder in water bottles (1 mg/mL, with mice consuming 5 mL/day per 25 g body weight). All study animals were sacrificed at 10 months of age with sodium pentobarbital (150 mg/kg, i.p.). Blood was drawn directly from the right atrium and perfused with 0.1 M PBS.

2.3. Sample collection

Blood was collected and centrifuged (2100 g for 10 min, 4 °C), and the plasma was kept at − 80 °C for biochemical analysis. Samples from the left lateral lobe of the liver and the left hemisphere of the brain were kept in 4% paraformaldehyde for 48 h to be processed for histological analysis. Additional liver samples and the right hemisphere of the brain were flash-frozen in liquid nitrogen and stored at − 80 °C until biochemical analysis.

2.4. Measurement of metabolites in plasma

Plasma levels of the hepatic enzymes glutamic oxaloacetic transaminase (GOT/AST) and glutamate pyruvate transaminase (GPT/ALT) were analyzed using commercial kits (Refs. DF43A and DF41A, respectively, Flex® reagent cartridge, Dimension, Siemens Healthcare GmbH, Erlangen, Germany) according to the manufacturer's instructions in a Siemens Dimension Vista 500 Lab System (Siemens Healthcare GmbH). In all cases, a calibration curve and internal controls were included in each assay. The plasma metabolites glucose (ref. 04404483190), urea (ref. 04460715190), creatinine (ref. 04810716190), triglycerides (TAGs, ref. 20767107322), total cholesterol (ref. 03039773190), HDL cholesterol (ref. 07528566190), LDL cholesterol (ref. 07005717190) were measured using commercial kits (Roche Diagnostics GmbH), according to the manufacturer's instructions, and a Roche/Hitachi cobas® Integra analyzer (Roche Diagnostics GmbH). The concentration of each metabolite was expressed in mg/dL. Liver enzyme levels were expressed in IU/L.

2.5. Plasma metabolite multiplex assays

Plasma levels of the metabolic hormones insulin, glucagon, ghrelin, leptin, glucagon-like peptide-1 (GLP-1), plasminogen activator inhibitor-1 (PAI-1), gastric inhibitory polypeptide (GIP) and resistin were determined by multiplex immunoassay system using commercial kits: Bio-Plex Pro™ mouse diabetes 8-plex immunoassay (Bio-Rad, Hercules, CA, USA, cat. Number: #171F7001M). Plasma levels of pituitary hormones growth hormone (GH), luteinizing hormone (LH), follicle-stimulating hormone (FSH), prolactin, adrenocorticotropic hormone (ACTH), brain-derived neurotrophic factor (BDNF), and thyroid-stimulating hormone (TSH) were determined by multiplex immunoassay system, using a commercial kit: MILLIPLEX MAP Mouse Pituitary Magnetic Bead Panel - Endocrine Multiplex Assay (Millipore Corporation, Billerica, MA, USA, cat. number: # MPTMAG-49 K). Plates were run on a Bio-Plex MAGPIX™ Multiplex Reader with Bio-Plex anager™ MP Software (Luminex, Austin, TX). Hormone concentrations were expressed in pg/mL, and detection limit was 68.29 (insulin), 0.50 (glucagon), 0.64 (ghrelin), 5.07 (leptin), 0.59 (GLP-1), 2.98 (PAI-1), 4.31 (GIP) and 184.89 (resistin), 1.70 (ACTH), 1.60 (BDNF), 9.50 (FSH), 1.70 (GH), 46.2 (prolactin), 1.90 (TSH) and 1.90 (LH) pg/mL, respectively.

2.6. Immunohistochemistry

Brain left hemisphere samples were post-fixed in 4% paraformaldehyde for 48 h and cryopreserved in 30% sucrose in 0.1 M PBS solution at 4 °C until processing. Coronal sections (30 μm) were cut with a cryostat (CM1950, Leica, Germany), collected, and stored in antifreeze solution (30% ethylene glycol, 20% glycerol in PBS) at − 20 °C until further used. Free-floating coronal sections containing the mouse hypothalamus and hippocampus were selected from − 1.22 to − 1.94 mm of Bregma levels [38]. For plaque amyloid-β analysis, we used rabbit anti-Aβ (1:500, Abcam, ab201060). Serial sections were washed in 0.1 M PBS for 5 min at room temperature three times and then blocked with 5% donkey serum, 0.5% Triton X-100 in 0.1 M PBS for 45 min at room temperature, as previously described [39]. Primary antibody diluted in 0.1 M PBS, 0.5% Triton X-100 (Sigma, #X-100), and 2.5% donkey serum (Sigma-Aldrich, St. Louis, MO, USA) was incubated overnight at room temperature. After rinsing, the sections were incubated with secondary antibody biotinylated goat anti-rabbit (1:500, GE Healthcare) diluted in 0.1 M PBS for 2 h at room temperature. All antibodies were diluted in PBS, 0.5% Triton X-100%, and 2.5% donkey serum (Sigma-Aldrich, St. Louis, MO, USA). We used the peroxidase-conjugated ExtraAvidin method and diaminobenzidine as the chromogen to visualize the reaction product of amyloid-β. For GFAP and IBA1 analysis, we used chicken anti-GFAP (1:1000, Abcam, #4674, lot GR3412062–1), respectively and goat anti-Iba1 (1:1000, Abcam, #Ab5076, lot GR3178750–2). Serial sections were washed in 0.01 M PBS for 5 min at room temperature three times and then blocked with 2% donkey serum (Jackson ImmunoResearch, #017–000–121, lot 143995), 0.3% Triton X-100 (Sigma, #X-100, lot 087K0086), 50 mM glycine (BIOSOLVE, #07132359) in 0.01 M PBS for 30 min at room temperature. Primary antibody diluted in PBS 0.01 M with 0.3% Triton X-100, 10 mM glycine, and 0.1% H_2O_2 was incubated overnight at room temperature. After rinsing, the sections were incubated with secondary antibody anti-chicken-AF488 (1:250, Jackson ImmunoResearch, #703–606–155, lot 143995) and anti-goat-HRP (1:250, Jackson ImmunoResearch, #705–035–147, lot 147415) diluted in 0.01 M PBS with 0.3% Triton X-100. After incubation, sections were washed 3 times with 0.01 M PBS and incubated in Cy3-TSA (1:250, Akoya Biosciences; part #TS-000202, lot 20203437) diluted in 1X Plus Amplification Diluent (Akoya Biosciences; #FP1135, lot 200120007) for 10 min at room temperature. Sections were then washed 3 times in 0.01 M PBS and incubated in PBS 0.01 M with 0.3% Triton X-100% and 3% H_2O_2 for 30 min at room temperature. Finally, slides were washed several times with 0.01 M PBS, counterstained with DAPI (4',6'-diamidino-2-phenylindol) (1:20000, Thermo Fisher Scientific, Cat#D1306; CAS: 28718–90–3) in 0.01 M PBS and mounted on gelatin-coated slides with ProLongTM Gold antifade reagent mounting medium (Invitrogen, #P36930, lot 2184477). Immunohistochemical images of amyloid-β were acquired with digital Camera DP70 (Olympus Iberia, S.A., Barcelona, Spain) connected to a microscope Olympus BX41. Fluorescent images were acquired with a confocal microscope (SP8, Leica, Germany), corrected for brightness and contrast, and analyzed using ImageJ software (http://imagej.nih.gov/ij), accessed on 24 March 2022). Images for quantification were taken at 20x. 3–4 sections per mouse were analyzed, with a total of 6 animals per group. DAPI was used to delimit the region of interest (ROI) of the following hypothalamic nuclei: arcuate nucleus (ARC), ventromedial nucleus (VMN), and paraventricular nucleus (PVN). The intensity of the GFAP signal and the area covered by GFAP staining was determined. For illustration purposes, representative images have been subjected to enhancements, including background subtraction as well as brightness and contrast adjustment.

2.7. RNA isolation and RT-qPCR analysis

We performed real-time PCR (TaqMan, ThermoFisher Scientific, Waltham, MA, USA) as described previously [40] using specific sets of primer probes from TaqMan® Gene Expression Assays as shown in Supplementary Table 1. Total RNA was extracted from hypothalamus and liver samples using the Trizol® method according to the manufacturer's instructions (ThermoFisher Scientific). RNA samples were isolated with RNAeasy minelute cleanup-kit including digestion with DNase I column (Qiagen) and quantified using a spectrophotometer to ensure A260/280 ratios of 1.8–2.0. After the reverse transcript reaction from 1 μg of mRNA, a quantitative real-time reverse transcription-polymerase chain reaction (qPCR) was performed in a CFX96TM Real-Time PCR Detection System (Bio-Rad, Hercules, CA, USA) and the FAM dye-labeled format for the TaqMan® Gene Expression Assays (ThermoFisher Scientific). A melting curve analysis was performed to ensure that only a single product was amplified. After analyzing several reference genes, values obtained from the hypothalamus and liver samples were normalized in relation to *Actb* levels (for further information, see Supplementary Table 1), which were found not to vary significantly between experimental groups.

2.8. Protein extraction and western blot analysis

Western blot analyses were performed as previously described [41,42] using corresponding primary antibodies as shown in Supplementary Table 2**.** Total protein from 5 to 15 mg of samples of the left lateral lobe of the liver was extracted for 30 min using 500 μL ice-cold cell lysis buffer (50 mM Tris-HCl pH 7.4, 150 mM NaCl, 0.5% NaDOC, 1 mM EDTA, 1% Triton, 0.1% SDS) supplemented with a cocktail of phosphatase (1 mM Na_3VO_4, 1 mM NaF) and protease inhibitors (cOmplete Tablets, Merck, Darmstadt, Germany). A quantity of 50 μg of protein was resolved on a 4–12% (Bis-Tris) Criterion XT Precast Gels (Bio-Rad Laboratories, Inc., Hercules, CA, USA, cat. number: 3450124), and then transferred onto nitrocellulose membranes (Bio-Rad Laboratories, Inc., Hercules, CA, USA). Total protein content was visualized after staining with Ponceau S red. Membranes were blocked in TBS-T (50 mM Tris-HCl pH 7.6, 200 mM NaCl, and 0.1% Tween 20) with 2% albumin fraction V from BSA (Roche, Mannheim, Germany) for 1 h at room temperature. To detect each targeted protein, the membrane was incubated overnight at 4ºC in TBS-T containing 2% BSA and the corresponding primary antibody (for further information, see Supplementary Table 2). Mouse γ-adaptin was used as the reference protein as previously described [42,43]. After several washes in TBS-T containing 1% Tween 20, an HRP-conjugated anti-rabbit or anti-mouse IgG (H+L) secondary antibody (Promega, Madison, WI, USA) diluted 1:10.000 was added followed by incubation for 1 h at room temperature. After extensive washing in TBS-T, the membranes were incubated for 1 min with the Western Blotting Luminol Reagent kit (Santa Cruz Biotechnology, Santa Cruz, CA, USA), and the specific protein bands were visualized and quantified by chemiluminescence using a Chemi-Doc TM MP Imaging System (Bio-Rad, Barcelona, Spain). To detect the phosphorylated form of proteins, after measuring phosphorylation proteins, the specific antibodies were removed from the membrane by incubation with stripping buffer (2% SDS, 62.5 mM Tris HCL pH 6.8, 0.8% ß-mercaptoethanol) 30 min at 50 °C. Membranes were extensively washed in ultrapure water, and then re-incubated with the corresponding antibody specific for the total protein. Quantification of results was performed using ImageJ software (http://imagej.nih.gov/ij). The results are expressed as either the phosphorylated form of target protein/target protein ratios or target protein/γ-adaptin ratios. Results for Non-Tg male protein levels were arbitrarily set as 1.

2.9. Liver histology

Liver samples were processed according to previously described protocols [44]. Briefly, samples from the left lateral lobe of the liver were post-fixed in 4% paraformaldehyde for 48 h and embedded in paraffin. Then, the paraffin blocks were sections into 5 μm-thick liver slices using a paraffin microtome. Subsequently, sections were deparaffinized and rehydrated through a series of xylene and alcohol baths, and then stained with hematoxylin-eosin (H-E) using a standard procedure for histological assessment of vacuole size and tissue status. Sections were mounted in aqueous mounting.

2.10. Total fat extraction in liver

Liver fat content was determined following previous standardized method [45]. Total lipids were extracted from frozen liver samples with chloroform-methanol (2:1, v/v) and butylated hydroxytoluene (0.025%, w/v) according to the Bligh and Dyer method. After two centrifugation steps (2800 g, 4 °C for 10 min), the lower phase containing lipids was isolated and dried by nitrogen. The liver fat content was expressed as a percentage of the tissue weight.

2.11. Measurement of food intake, body weight, energy expenditure and respiratory quotient

Food intake and body weight were measured weekly during treatment. After 3 months of DCI administration, mice were placed in metabolic cages and energy expenditure (EE, kcal/kg lean mass) and respiratory quotient (RQ, VCO_2/VO_2) were analyzed for 48 h using a calorimetric system (LabMaster, TSE System, Bad Homburg, Germany) as previously described [46]. This system is an open-circuit instrument that determines: (1) the energy consumed by the amount of caloric intake (kilocalories) over time (hours) and normalized by the lean mass (kilograms) and (2) the ratio of CO_2 production to O_2 consumption (VCO_2/VO_2). The activity was measured by an infrared system that counts mouse movement and rearing. Previously, all mice were acclimated to the experimental room and habituated to the cage system for 48 h before starting the measurements.

2.12. Spontaneous alternation Y-maze test

Working memory was evaluated by spontaneous alternation behavior [47]. Each mouse was initially placed within one arm of the maze (40 ×4.5 ×14 cm, made of gray Plexiglas), and allowed to explore the maze for 8 min. Illumination was provided with a maximum light intensity in the center of the maze of 100 lux. The sequence of alternation and the number of arm entries (when the hind limbs had completely entered the arm) were assessed. A correct trial was defined as entering the output arm without entering other arms. The percentage of spontaneous alternation behavior was calculated for each animal as follows: [(Number of correct trials)/(Total arm entries – 2)] × 100 [48]. Animals were tested in the Y-maze before and during DCI treatment (after two months of treatment) to address the effect of DCI on the progressive decline of working memory.

2.13. Morris water maze (MWM)

Morris water maze was used to study learning and memory [49]. The maze consisted of a circular pool (120-cm diameter and 0.6 m height) filled with nontoxic opaque water (up to 0.4 m) at 23 ± 2ºC temperature and virtually subdivided into four equal quadrants (Q1-Q4). The escape platform (10-cm diameter) was raised 0.5 cm above the water surface for visual learning. The hidden platform was located 0.5 cm below the water surface for acquisition and reversal spatial learning. To aid the mice in orienting themselves concerning the pool, the room testing was decorated with eye-catching visual cues.

We assessed the following behavioral learning procedure: in habituation training mice received 2 trials for one day and were allowed to explore the pool freely for 60 s. The pool was virtually subdivided into

distinct zones: peripheral (20 cm from walls), intermediate (20–50 cm from walls) and center (50 cm from walls) to evaluate the amount of time spent in the respective area of each animal [50]. In visual learning, mice received 4 trials for two days (30-min intertribal intervals). The trial ended when the mouse climbed into the visible escape platform, or after a maximum trial duration of the 60 s. If a mouse did not find the escape platform during a trial, it was placed on the platform for 10 s. The location of the platform and the starting point of animals were changed in each trial. In acquisition spatial learning, animals received 6 trials for four days (30-min intertribal intervals). The hidden platform was placed on quadrant 1 (Q1) during all training. The starting point of mice was changed in each trial. The maximum duration of the trial was 60 s unless the mouse reached the hidden platform. In reversal spatial learning, the hidden escape platform was positioned in a new position (opposite to its placement on acquisition learning, quadrant 3 (Q3)) and mice received 6 trials for one day (30-min intertribal intervals). We examined escape latency on each occasion.

2.14. Statistical analysis

Data were analyzed using the R statistical software package, version 3.6.2 (http:www.r-project.org/) and Graph-Pad Prism 7.0 software, including principal component analysis (PCA), multiple linear regression analysis and multiple correlations with hierarchical clustering based on Euclidean distance matrixes. Values are represented as mean ± standard error of the mean (SEM) for each experimental group, according to the assay. The significance of differences within and between groups was evaluated by a three-way analysis of variance (ANOVA), whose factors were "genotype", "treatment" and "sex"; followed by Tukey post-hoc test for multiple comparisons. Alternatively, baseline comparisons were evaluated by a two-way ANOVA, whose factors were "genotype" and "sex", followed by Tukey post-hoc test. A *p*-value $p < 0.05$ was considered statistically significant as it is generally assumed. (* $p < 0.05$; ** $p < 0.01$; *** $p < 0.001$) represent non-Tg versus 5xFAD, in the same-sex, same-genotype untreated group. (^$p < 0.05$; ^^$p < 0.01$; ^^^$p < 0.001$) represent untreated versus DCI-treated mice in the same-sex, same-treatment group.

3. Results

3.1. DCI increased food intake and reduced weight loss in the 5xFAD mice

Previous studies have shown that 5xFAD mice exhibit decreased food intake patterns and weight loss starting at 6 months of age, which is associated with decreased hypothalamic insulin signaling [10,51]. The effect of DCI supplementation for 4 months on body weight and food intake from 6 months of age was determined. Both male and female 5xFAD mice showed an initial decrease in body weight ($p < 0.01$ for males, $p < 0.001$ for females) (Fig. 1A), and showed a successive weight loss 4 months later (month 4: $p < 0.05$ for 5xFAD females vs. non-Tg females). These effects were attenuated by DCI administration (month 2: $p < 0.01$ for treated vs. non-treated 5xFAD females; month 4: $p < 0.05$ for both male and female treated mice) (Fig. 1B, C).

Both male and female 5xFAD mice showed a decrease in cumulative food intake ($p < 0.001$ for both males and females at week 14) (Fig. 1D, E), which was similar to that of non-Tg littermates when normalized by body weight (Fig. 1F-G), providing evidence that weight loss occurs gradually due to low caloric intake. DCI treatment significantly increased food intake in male and female 5xFAD mice ($p < 0.001$ in males; $p < 0.01$ in females at week 14) (Fig. 1D, E), as well as food intake by body weight, being more evident in male 5xFAD mice ($p < 0.001$ in males; $p < 0.05$ in females at week 14 (Fig. 1F).

Analysis of food intake normalized by body weight (BW) over 48 h in metabolic cages showed decreased food intake during the early and mid-hours of the night for both male and female 5xFAD mice that were attenuated by DCI administration (Supplementary Figures 1A, B). Furthermore, we found a significant genotype effect on mean daily food intake during day ($F_{1,34} = 15.39$, $p < 0.001$), at night ($F_{1,34} = 15.39$, $p < 0.001$) and throughout the whole day ($F_{1,34} = 15.90$, $p < 0.001$), which was attenuated by DCI treatment as observed by genotype x treatment interaction during the day ($F_{1,34} = 3.89$, $p < 0.05$), at night ($F_{1,34} = 4.011$, $p < 0.05$) and overall ($F_{1,34} = 3.948$, $p < 0.05$). 5xFAD males showed decreased food intake as compared to non-Tg males during the day and overall ($p < 0.05$ for both), whereas 5xFAD females showed a similar trend in overall 24 h food intake when compared to non-Tg females ($p < 0.05$). The distribution of food intake during the day and night was not significantly affected by either genotype or treatment (Supplementary Figure 1F). No significant differences were observed between DCI-treated 5xFAD mice and non-Tg mice, depicting normalized food intake behavior.

Analysis of drink consumption normalized by body weight showed a significant genotype effect in total water consumed over 24 h ($F_{1,52} = 8.705$, $p < 0.01$) and a significant DCI effect as observed by genotype x treatment interaction ($F_{1,52} = 3.906$, $p < 0.05$), depicting also lower overall water intake in 5xFAD mice, which was normalized by DCI treatment (Supplementary Figures 1G-J). This effect was more pronounced in females as there was a specific significant difference between 5xFAD females and non-Tg females ($p < 0.05$) (Supplementary Figure 1I). Again, the distribution of drink consumption during the day and night was not significantly affected by genotype or DCI treatment (Supplementary Figure 1J) in agreement with the food intake.

Since body weight reduction and weight loss could affect the whole energy metabolism, we determined the energy expenditure (EE) and respiratory quotient (RQ) of 5xFAD mice (Fig. 1H-K). There was a significant genotype effect in EE per body weight (EE/BW) during the day ($F_{1,43} = 6.519$, $p < 0.01$) and night ($F_{1,43} = 5.185$, $p < 0.01$), but only 5xFAD females showed reduced EE/BW in light and dark phases ($p < 0.05$ for all) when specifically compared to Non-Tg females (Fig. 1L, M). DCI-treated 5xFAD females had normal EE/BW as compared to non-Tg. DCI significantly increased EE/BW in 5xFAD females during the dark phase ($p < 0.05$) (Fig. 1J, M). The activity was analyzed in parallel to energy expenditure (Supplementary Figures 1K-N) and showed a significant sex x genotype interaction during the night ($F_{1,48} = 5.275$, $p < 0.05$) (Supplementary Figure 1 M), suggesting lower activity in female 5xFAD mice in agreement with the measurement of lower energy expenditure.

RQ indicates the rate of glucose or fat fuel utilization, as lower RQ measurements correlate with higher O_2 consumption in lipid β-oxidation. There was a significant genotype effect on RQ during the day ($F_{1,45} = 7.421$, $p < 0.01$) and night ($F_{1,45} = 7.183$, $p < 0.05$), and both male and female 5xFAD mice showed decreased RQ during light and dark phases ($p < 0.05$ for all), whereas DCI only normalized RQ in female 5xFAD mice ($p < 0.05$ vs non-treated 5xFAD females) (Fig. 1N, O). These results suggest 5xFAD mice reduced their EE to offset the decreased nutrient disposal due to low food intake and tended to use fat as fuel, leading to decreased adiposity. Preliminary data of our group by bioimpedance spectroscopy analysis suggested a decrease in fat tissue of 5xFAD animals.

Metabolic alterations in 5xFAD mice were accompanied by deficits in hippocampal-dependent spatial working memory as assessed by the Y-maze test. Both male and female 5xFAD mice displayed working memory impairments starting at 6 months of age compared to their sex-matched non-Tg littermates ($p < 0.01$ and $p < 0.05$ respectively) (Supplementary figures 2A, B), while only males showed a higher number of compulsion-related arm entries ($p < 0.01$) (Supplementary Figures 2C-E). At 8 months of age, DCI specifically improved alternation performance in males, but not in females, as demonstrated by the significant treatment effect ($F_{1,25} = 6.138$, $p < 0.05$) and interaction ($F_{1,25} = 7.868$, $p < 0.01$). Single comparisons showed greater differences in working memory performance in untreated 5xFAD mice ($p < 0.001$) than in DCI-treated 5xFAD mice ($p < 0.05$) as compared to their non-Tg male littermates (Supplementary Figures 2A, B). Although there was no DCI

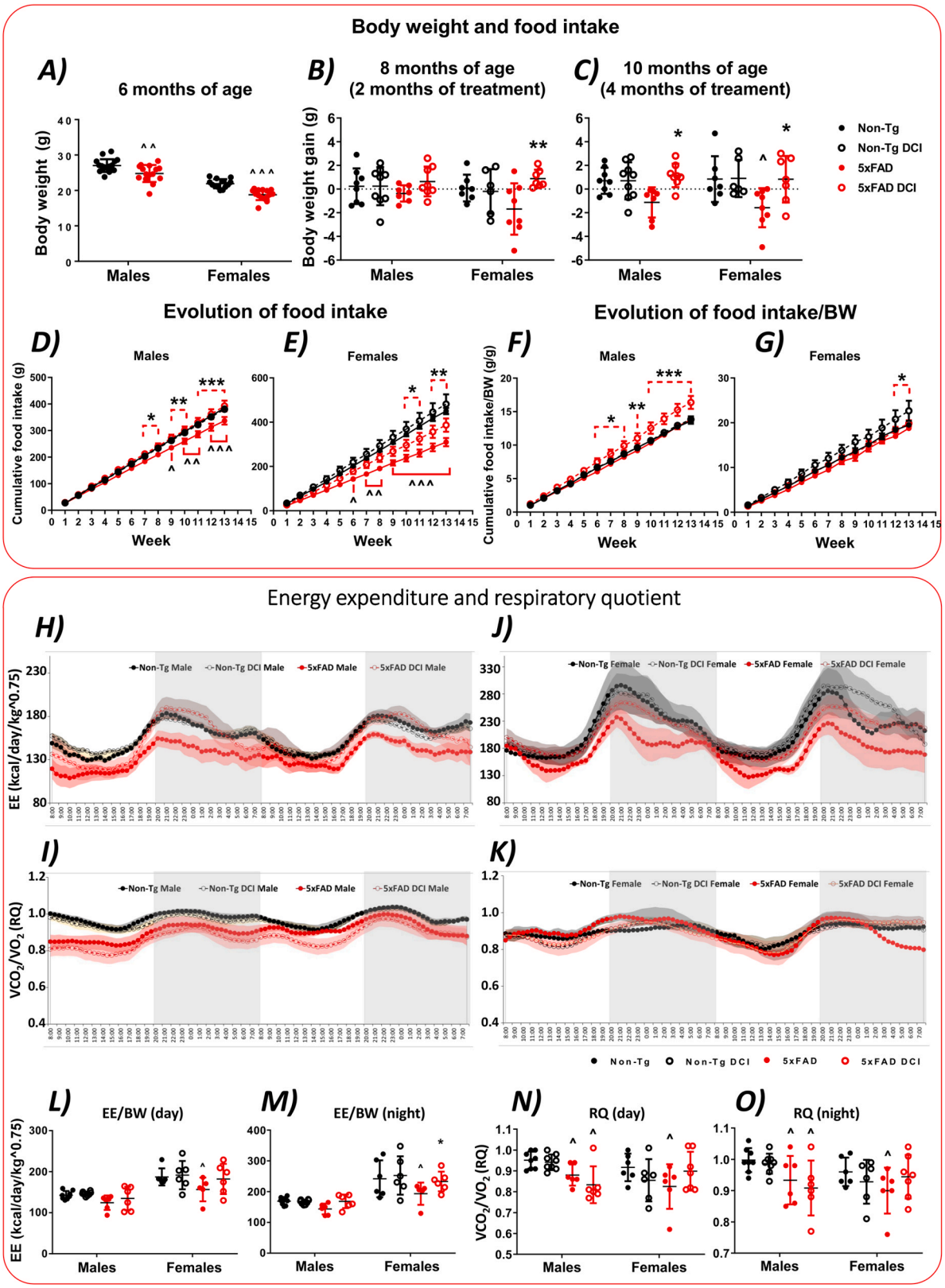

Fig. 1. Effect of DCI on body weight, food intake and energy expenditure after 4 months of treatment in male and female 5xFAD mice. A) Body weight was measured at the beginning of the treatment. B-C) Body weight difference respect to beginning of treatment after 2 months and at the end of the treatment at 4 months prior to tissue collection. D-G) Cumulative food intake was determined weekly and represented as total grams of food consumed and grams of food per grams of body weight. H-K) Energy expenditure (EE) normalized per total body weight (BW) and respiratory quotient (RQ) calculated as vO_2/vCO_2 ratio after 3 months of treatment. L-O) Mean EE/BW and RQ during day and night in 48 h of measurement. N = 6–9 per group. Three-way ANOVA analysis (sex x genotype x treatment) with Tukey's post hoc test; significant differences between same-treatment non-Tg versus 5xFAD: * = $p < 0.05$, ** = $p < 0.01$, *** = $p < 0.001$; significant differences between same-genotype control versus DCI-treated: ^ = $p < 0.05$, ^^ = $p < 0.01$, ^^^ = $p < 0.001$.

effect in number of arm entries, only untreated 5xFAD males showed significant differences from non-Tg males as determined by Tukey post-hoc test ($p < 0.01$) (Supplementary Fig. s2C-E).

Along with working memory, animals underwent MWM test to assess specific changes in hippocampal-dependent reference memory, place memory and cognitive flexibility, determined by the latency to reach the platform in the visual, acquisition, and reversal phases of MWM, respectively (Supplementary Figures 2F-H) [52]. Overall, female mice showed longer latency to reach the platform as shown by a sex effect (F_{3360} =89.42, $p < 0.001$). Both 5xFAD males and females exhibited a longer latency to escape the platform in the visual and acquisition phases compared to their non-Tg littermates. 5xFAD males also showed a longer latency to the platform in the inversion phase specifically in males (Supplementary Figures 2G, H). DCI-treated 5xFAD males showed improved performance in the inversion phase compared to untreated 5xFAD males ($p < 0.01$ in all assays), demonstrating greater cognitive flexibility (Supplementary Figure 2G). These results suggest that DCI treatment attenuates cognitive decline in visuospatial tasks requiring both working and plasticity, specifically in males.

3.2. DCI attenuated sex-specific differences in plasma hormones and metabolites in 5xFAD mice

We assessed plasma levels of metabolites (Table 1), metabolic hormones (Fig. 2A-H) and pituitary hormones (Fig. 1I-O) in 5xFAD mice. As previously described, 5xFAD mice show early deficits of fasting insulin and insulin secretagogues [10]. Because DCI has been shown to enhance insulin signaling, we determined its effect on 10-month old 5xFAD mice. Notably, we found a genotype effect showing lower TAGs ($F_{1,46}$ =4.30, $p < 0.05$) and cholesterol ($F_{1,46}$ =6.91, $p < 0.05$) levels in 5xFAD mice, but higher GPT levels ($F_{1,46}$ =7.69, $p < 0.01$) (Table 1). There was a significant genotype x treatment interaction for most metabolites, showing a decrease in glucose, GPT, GOT, uric acid, and HDL levels, whereas TAGs, cholesterol, and LDL levels were increased (Table 1). Individual comparisons showed a specific increase in the liver damage markers GOT and GPT ($p < 0.01$ for both) in 5xFAD females compared to non-Tg females, but not in 5xFAD females treated with DCI, which showed a decrease in uric acid and GOT levels compared to untreated 5xFAD females ($p < 0.05$ for both) (Table 1).

Insulin secretion is enhanced by GLP-1 and GIP to control the post-prandial plasma glucose elevation levels. Both hormones regulate food intake and energy homeostasis, while PAI-1 is related to plasma insulin levels [53]. There was a significant genotype effect as a result of lower plasma levels of insulin ($F_{1,52}$ =17.38, $p < 0.001$), GIP ($F_{1,52}$ =10.43, $p < 0.001$), GLP-1 ($F_{1,52}$ =4.23, $p < 0.05$) and PAI-1 ($F_{1,52}$ =5.309, $p < 0.05$) in 5xFAD mice. A significant genotype x treatment interaction was observed for insulin ($F_{1,52}$ =6.477, $p < 0.05$) and GIP ($F_{1,52}$ =6.466, $p < 0.05$) showing that DCI treatment normalized deficient insulin secretion. Tukey single comparisons depicted significant differences between male 5xFAD mice and their non-Tg littermates for insulin ($p < 0.05$), GIP ($p < 0.05$) and PAI-1 ($p < 0.05$), while 5xFAD females showed a similar trend for insulin ($p < 0.001$), GIP ($p < 0.05$), and GLP-1 ($p < 0.05$) (Fig. 2A-H). Resistin and leptin are released by white adipose tissue, and their overexpression is related to inflammatory responses in obesity. There was also a significant sex-specific difference in resistin plasma levels ($F_{1,52}$ =21.13, $p < 0.001$), showing a sex x genotype interaction as a result of increased resistin levels in 5xFAD males but reduced levels in 5xFAD females compared to their non-Tg littermates ($F_{1,52}$ =10.75, $p < 0.01$).

Pituitary hormone release is regulated by hypothalamic and external neuroendocrine signaling. When determining pituitary hormones in plasma, sex x genotype interactions were observed for ACTH, GH, TSH, FSH, and BDNF. DCI treatment x genotype interactions were significant only for prolactin and BDNF levels, evidencing an effect of DCI on gonadotropins controlling sex hormone production in 5xFAD mice. Single comparisons showed an increase in FSH levels in 5xFAD females ($p < 0.001$), suggesting an age-related loss of fertility.

Principal component analysis (PCA) showed that plasma metabolites and hormones were differently influenced by sex, genotype and DCI treatment. Principal Component 1 (PC1) accounted for 37.15% of the variance (factor loads of at least ± 0.4 per variable: resistin 0.588, leptin −0.372, BDNF 0.705, total cholesterol −0.794, glucose 0.442, GOT 0.492, GPT 0.481, HDL −0.785, TAGs −0.655, GH −0.594, THS −0.789, prolactin 0.687, FSH −0.746, ACTH −0.660) and PC2 comprised 25.28% of the variance (factor loads of at least ± 0.4 per variable: GIP −0.631, GLP-1 −0.481, insulin −0.601, glucose 0–457, creatinine 0.442, GPT 0.545, GPT 0.418, uric acid 0.460) (Fig. 2P-R). 5xFAD males were clustered separately from non-Tg mice based on PC1, (Fig. 2Q), whereas 5xFAD females were separated from non-Tg mice on PC2 distribution (Fig. 2R). DCI-treated male and female 5xFAD mice were clustered together with the non-Tg mice, showing normalization of atypical plasma parameters (Fig. 2Q, R). These graphs indicate that pituitary hormonal imbalance was the main component that separated 5xFAD male mice, whereas insulin signaling and hepatic and renal metabolites contributed largely to the separation of 5xFAD females. This is a key finding that suggests that sex differences modulate the impact of the transgene-derived elevation of Aβ, providing a new study framework for human AD.

3.3. Hypothalamic expression of neuroendocrine regulators of food intake and body weight is differently affected by sex and genotype and is ameliorated by DCI treatment

Whole-body energy homeostasis is precisely regulated by the hypothalamus, compensating for food intake and energy expenditure. Thus, we determined the relative expression of genes involved in short and long-term orexigenic (*Npy*, *Agrp, Galp*) and anorexigenic (*Pomc*, *Cartpt*) responses, circadian-regulated appetite patterns (*Hcrt*, *Pmch*), exercise-induced responses in food intake and energy expenditure (*Fndc5*), along with hypothalamic paracrine expression of metabolic peptides and receptors (Fig. 3A-T). There was a main effect of genotype as a result of a decreased expression of *Npy* ($F_{1,49}$ =4.507, $p < 0.05$), *Pomc* ($F_{1,49}$ =14.79, $p < 0.001$), *Cartpt* ($F_{1,49}$ =13.15, $p < 0.001$), *Hcrt* ($F_{1,49}$ =19.59, $p < 0.001$), *Pmch* ($F_{1,49}$ =25.49, $p < 0.001$), Fndc5 ($F_{1,49}$ =7.183, $p < 0.01$) and *Galp* ($F_{1,49}$ =6.701, $p < 0.05$), while the marked decrease in *Pomc* was male-specific (sex x genotype interaction: $F_{1,49}$ =6.264, $p < 0.05$). DCI treatment increased the expression of *Npy* ($F_{1,49}$ =13.69, $p < 0.001$), *Agrp* ($F_{1,49}$ =10.78, $p < 0.01$) and *Pmch* ($F_{1,49}$ =6.386, $p < 0.05$) independently of sex and genotype, while DCI promoted *Pomc* expression in 5xFAD mice (genotype x treatment interaction: $F_{1,49}$ =4.767, $p < 0.05$) and *Galp* expression specifically in females (sex x treatment interaction: $F_{1,49}$ =23.39, $p < 0.001$). These results suggest that hypothalamic dysfunction is generalized in 5xFAD mice, losing appetite control through neuropeptide signaling, whereas DCI treatment is effective in increasing orexigenic signaling but does not restore the widespread loss of hypothalamic neuropeptide expression.

Along with the loss of neuropeptide expression, there was a significant effect of genotype on the decrease in insulin receptor (*Insr*) expression ($F_{1,49}$ =7.606, $p < 0.001$). However, the hypothalamus of 5xFAD mouse exhibited an overall decrease in ghrelin (*Ghrl*) expression ($F_{1,49}$ =11.68, $p < 0.01$) and an increase in pre-proglucagon peptide (*Gcg*) ($F_{1,49}$ =8.101, $p < 0.01$) and IGF-1 (*Igf1*) ($F_{1,49}$ =26.92, $p < 0.001$) expression. There was a sex x genotype interaction showing increased resistin (*Retn*) expression in males, while decreased in 5xFAD females ($F_{1,49}$ =8.153, $p < 0.01$), and the opposite for GnRH (*Gnrh1*) ($F_{1,49}$ =9.247, $p < 0.01$). In this case, DCI treatment specifically increased hypothalamic insulin (*Ins2*) expression in 5xFAD females (sex x genotype x treatment interaction: $F_{1,49}$ =5.135, $p < 0.05$), but inversely reduced *Igf1* (sex x genotype x treatment interaction: $F_{1,49}$ =4.005, $p < 0.05$). These results suggest that DCI appears to improve insulin signaling in the hypothalamus.

Since hypothalamic inflammations have already been observed in

Table 1
Effect of DCI on biochemical parameters in the plasma of male and female 5xFAD mice [1].

	Males				Females				Three-way ANOVA						
	Non-Tg	Non-Tg DCI	5xFAD	5xFAD DCI	Non-Tg	Non-Tg DCI	5xFAD	5xFAD DCI	Sex	Genotype	Treatment	S x G	S x T	G x T	S x G x T
Triglycerides (mg/dL)	125.66 ± 8.37	103.29 ± 6.85	81.54 ± 8.40^	108.61 ± 16.72	87.70 ± 16.78	73.34 ± 8.25	63.80 ± 6.37	74.07 ± 7.76	$F_{1,46}$ = 14.73 P < 0.001	$F_{1,46}$ = 4.30 P < 0.05	ns	ns	ns	$F_{1,46}$ = 4.22 P < 0.05	ns
Total Cholesterol (mg/dL)	80.74 ± 1.99	89.56 ± 4.84	77.22 ± 2.85	71.14 ± 4.11	58.05 ± 2.30	59.94 ± 3.23	59.88 ± 2.31	54.46 ± 2.65	$F_{1,46}$ = 76.79 P < 0.001	$F_{1,46}$ = 6.91 P < 0.05	ns	ns	ns	$F_{1,46}$ = 5.23 P < 0.05	ns
HDL (mg/dL)	37.48 ± 1.32	34.26 ± 2.54	33.84 ± 2.96	23.49 ± 3.19	20.72 ± 1.60	15.94 ± 3.76	21.82 ± 1.15	19.19 ± 2.63	$F_{1,46}$ = 51.16 P < 0.001	ns	ns	$F_{1,46}$ = 7.81 P < 0.01	$F_{1,46}$ = 7.11 P < 0.01	ns	Ns
LDL (mg/dL)	21.20 ± 1.93	29.24 ± 2.77	27.07 ± 3.60	23.44 ± 2.15*	19.80 ± 4.12	29.18 ± 3.56	20.00 ± 1.02	22.66 ± 3.43	ns	ns	ns	ns	ns	$F_{1,46}$ = 4.46 P < 0.05	ns
Urea (mg/dL)	62.75 ± 6.71	66.13 ± 5.37	54.60 ± 5.53	65.96 ± 6.12	82.52 ± 6.04	65.76 ± 3.88	74.40 ± 5.96	66.30 ± 5.98	$F_{1,46}$ = 5.50 P < 0.05	ns	ns	ns	ns	$F_{1,46}$ = 5.03 P < 0.05	ns
Uric acid (mg/dL)	2.36 ± 0.46	2.23 ± 0.38	2.68 ± 0.83	2.30 ± 0.45	2.63 ± 0.50	3.57 ± 1.45	5.50 ± 1.27	2.27 ± 0.43*	$F_{1,46}$ = 4.39 P < 0.05	ns	ns	ns	ns	$F_{1,46}$ = 5.07 P < 0.05	ns
Creatinine (mg/dL)	0.51 ± 0.03	0.39 ± 0.03	0.37 ± 0.02	0.36 ± 0.07	0.34 ± 0.02	0.40 ± 0.03	0.44 ± 0.05	0.36 ± 0.05	ns	ns	ns	ns	ns	ns	$F_{1,46}$ = 4.13 P < 0.05
Glucose (mg/dL)	206.96 ± 14.53	208.30 ± 13.08	231.50 ± 12.36	186.66 ± 11.81	157.33 ± 6.84	188.60 ± 19.18	204.80 ± 20.24	160.76 ± 18.62	$F_{1,46}$ = 8.28 P < 0.01	ns	ns	ns	ns	$F_{1,46}$ = 8.22 P < 0.01	ns
GPT (U/L)	53.10 ± 6.37	76.51 ± 8.72	65.88 ± 11.56	63.26 ± 10.20	71.95 ± 12.09	103.80 ± 14.72	175.00 ± 30.49^^	126.67 ± 25.47	$F_{1,46}$ = 22.84 P < 0.001	$F_{1,46}$ = 7.69 P < 0.01	ns	$F_{1,46}$ = 7.00 P < 0.05	ns	$F_{1,46}$ = 4.89 P < 0.05	ns
GOT (U/L)	233.48 ± 41.17	278.88 ± 36.02	259.08 ± 78.26	235.36 ± 29.71	331.67 ± 80.12	566.00 ± 146.46	986.88 ± 318.17^^	430.40 ± 70.19*	$F_{1,46}$ = 21.55 P < 0.001	ns	ns	ns	ns	$F_{1,46}$ = 7.62 P < 0.01	$F_{1,46}$ = 5.37 P < 0.05

[1]N = 6–9 per group. Three-way ANOVA analysis (sex x genotype x treatment) with Tukey's post hoc test; significant differences between same-treatment non-Tg versus 5xFAD: * = $p < 0.05$, ** = $p < 0.01$, *** = $p < 0.001$; significant differences between same-genotype control versus DCI-treated: ^ = $p < 0.05$, ^^ = $p < 0.01$, ^^^ = $p < 0.001$.

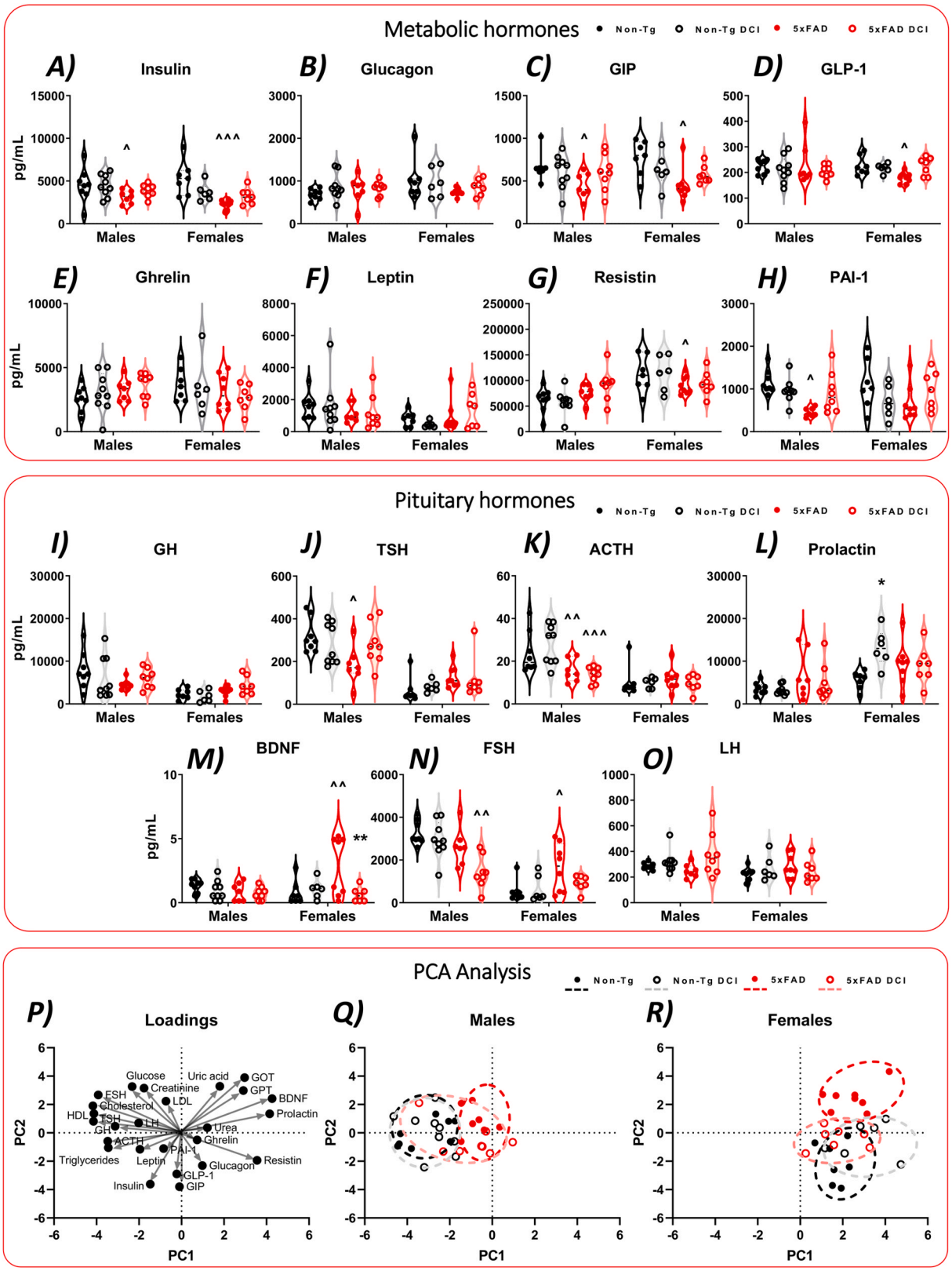

Fig. 2. Effect of DCI on the plasma levels of metabolic and pituitary hormones in male and female 5xFAD mice. A-H) Measurement of insulin, glucagon, gastric inhibitory polypeptide (GIP), glucagon-like-peptide 1 (GLP-1), ghrelin, leptin, resistin and plasma plasminogen activator inhibitor-1 (PAI-1) in plasma. I-O) Measurement of growth hormone (GH), thyroid-stimulating hormone (TSH) adrenocorticotropic hormone (ACTH), prolactin, brain-derived neurotrophic factor (BDNF), follicle-stimulating hormone (FSH) and luteinizing hormone (LH) in plasma. P-R) Principal component analysis of plasma hormones and metabolites showing factor loadings and component separation in non-Tg and 5xFAD mice. N = 6–9 per group. Three-way ANOVA analysis (sex x genotype x treatment) with Tukey's post hoc test; significant differences between same-treatment non-Tg versus 5xFAD: * = $p < 0.05$, ** = $p < 0.01$, *** = $p < 0.001$; significant differences between same-genotype control versus DCI-treated: ^ = $p < 0.05$, ^^ = $p < 0.01$, ^^^ = $p < 0.001$.

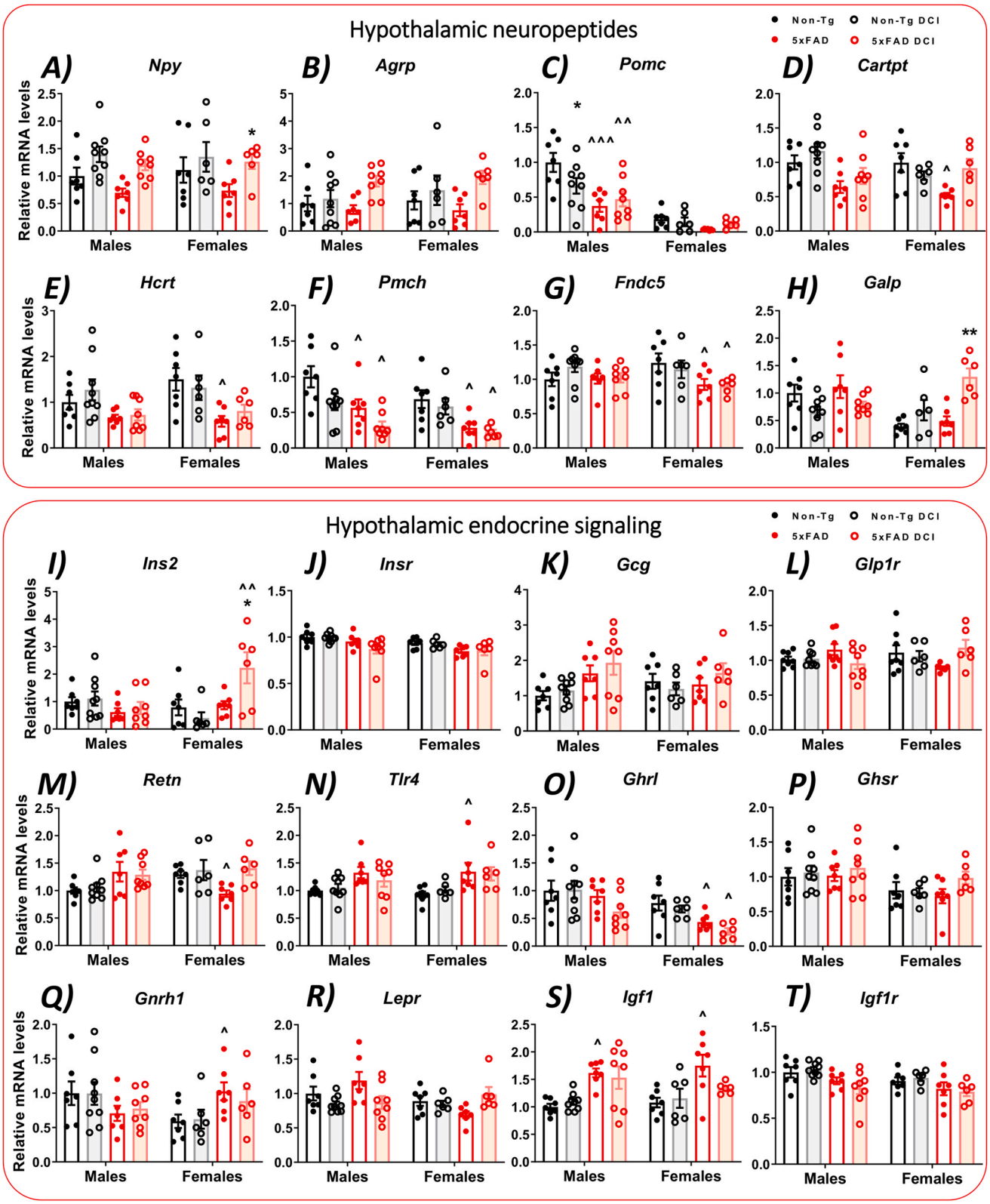

Fig. 3. Effect of DCI on orexigenic and anorexigenic neuropeptides and endocrine signaling factors in the hypothalamus of male and female 5xFAD mice. A-H) Gene expression of the hypothalamic neuropeptide Y (*Npy*), agouti-related peptide (*Agrp*), pro-opiomelanocortin (*Pomc*), cocaine and amphetamine-regulated transcript prepropeptide (*Cartpt*), orexin (hipocretin; *Hcrt*), pre-melanin concentrating hormone (*Pmch*), irisin precursor fibronectin type III domain-containing protein 5 (*Fndc5*), galalnin-like peptide (*Galp*). I-T) Gene expression in the hypothalamus of endocrine markers insulin (*Ins2*), insulin receptor (*Insr*), Preproglucagon (*Gcg*), glucagon-like peptie 1 receptor (*Glp1r*), resistin (*Retn*), Toll-like receptor 4 (Tlr4), ghrelin (*Ghrl*), growth hormone secretagogue receptor (*Ghsr*), gonadotropin-releasing hormone 1 (*Gnrh1*), leptin receptor (*Lepr*), insulin-like growth factor (*Igf1*) and Igf1 receptor (*Igf1r*). N = 6–9 per group. Three-way ANOVA analysis (sex x genotype x treatment) with Tukey's post hoc test; significant differences between same-treatment non-Tg versus 5xFAD: * = $p < 0.05$, ** = $p < 0.01$, *** = $p < 0.001$; significant differences between same-genotype control versus DCI-treated: ^ = $p < 0.05$, ^^ = $p < 0.01$, ^^^ = $p < 0.001$.

3xTg and 5xFAD mouse models of AD [10,54–57] and appear to contribute to defective hypothalamic control of energy homeostasis, we sought to determine the impact of neuroinflammation in 5xFAD mice and the ability of DCI to prevent it. Overall, main we observed a main effect of genotype indicating that 5xFAD mice had higher hypothalamic expression of TNF-α (*Tnf*) ($F_{1,49}$ =18.38, $p < 0.001$), IL-1β (*Il1b*) ($F_{1,49}$ =82.55, $p < 0.001$), GFAP (*Gfap*) ($F_{1,49}$ =80.01, $p < 0.001$) and IBA1 (*Aif1*) ($F_{1,49}$ =23.93, $p < 0.001$), the latter being mainly driven by males (sex x genotype interaction: $F_{1,49}$ =4.535, $p < 0.05$). As with *Igf1*, DCI exerted its effect on reducing *Gfap* expression specifically in 5xFAD females (sex x genotype x treatment interaction: $F_{1,49}$ =7.498, $p < 0.01$), and DCI-treated 5xFAD females had lower *Gfap* expression when compared to control 5xFAD females ($p < 0.001$). However, no significant effect of genotype was observed on other markers of inflammation or astrocyte reactivity such as IL-6 (*Il6*), NF-κB (*Nfkb1*), or S100b (*S100b*), or markers related to cell death such as caspase 3 (*Casp3*). Interestingly, although the *Il6* response was not upregulated, DCI treatment caused a reduction of its expression specifically in 5xFAD mice (genotype x treatment interaction: $F_{1,49}$ =5.009, $p < 0.05$). These results suggest that hypothalamic inflammation is dependent on *Tnf, Il1b and Gfap*, whereas DCI seems to decrease GFAP response in a sex-dependent manner, more preeminently in females.

Thus, inflammation could be related to alterations in gene expression of neuropeptides and endocrine signals in the hypothalamus regulating food intake and body weight. To assess this, correlations were performed across all genes and the hierarchical organization distributed clusters of significantly interrelated genes in both males and females (Supplementary Figures 3A, B). The clusters showed a significant negative correlation between *Il1b, Tnf, Gfap and Igf1* with *Npy, Agrp, Pomc, Cartpt, Hcrt, Pmch, Fndc5, and Ghrl.*

Given these results, multiple linear regression analysis was performed to assess whether reduced food intake (FI) or body weight (BW) were associated with altered expression of neuropeptide- or inflammation-related genes (Fig. 4I-M). In males, a significant positive correlation (spearman ρ) was found between FI and the orexigenic neuropeptides *Npy* and *Agrp* ($p < 0.05$ for all), whereas BW was related to *Cartpt, Pomc, Fndc5, and Ghrl* ($p < 0.05$ for all). Significant negative correlations were found between FI and Igf1, Il1b ($p < 0.05$ for both), Gfap ($p < 0.01$), and *Tnf* ($p < 0.001$), while a similar trend was observed for BW and *Igf1*, *Il1b*, *Gfap* ($p < 0.05$), *Tnf* ($p < 0.001$) and this time, also *Gcg* ($p < 0.01$). In females, however, significant positive correlations were found between FI and *Npy*, *Agrp*, *Pomc*, *Pmch* ($p < 0.05$ for all), *Retn* ($p < 0.01$), *Hcrt* ($p < 0.001$), similarly to BW, where significant associations were found for *Pomc*, *Pmch*, and also *Cartpt*, *Fndc5* and *Ghrl* ($p < 0.05$ for all). Strong negative associations were found for *Ilb* and *Gfap* with FI and BW ($p < 0.001$ for all), and also for *Igf1* ($p < 0.01$ for FI; $p < 0.05$ for BW) and *Tlr4* ($p < 0.05$ for both). FI was also negatively associated with *Ins2* ($p < 0.05$), while BW was also negatively associated with *Gnrh1* ($p < 0.05$).

These results together show a sex-differentiated model of metabolic dysfunction, in which hypothalamic inflammation contributes to altered signaling in the hypothalamus. DCI promotes food intake and prevents weight loss by increasing orexigenic drive by *Npy* and *Agrp* expression, but also specifically in females by decreasing pro-inflammatory expression of *Gfap* and *Igf1* (Fig. 4I).

3.4. Hypothalamic astrogliosis is sex and nuclei-dependent in 5xFAD mice

Since *Gfap* mRNA expression was significantly increased and associated with changes in hypothalamic neuropeptide expression, GFAP immunofluorescence was performed to determine astrogliosis in specific hypothalamic nuclei of 5xFAD and its response to DCI. Given that hypothalamic *Aif1* expression was also elevated in 5xFAD males, we additionally performed immunofluorescence analysis of IBA1 staining to determine changes in the microglial number and/or dimension. GFAP and IBA1 signal intensities and areas covered in the arcuate nucleus (ARC), ventromedial nucleus (VMN), and paraventricular nucleus (PVN) of the hypothalamus were analyzed (Fig. 5A-G) (Supplementary Figures 4A-G).

We observed a significant genotype effect on GFAP immunofluorescence in the ARC ($F_{1,40}$ =10.10, $p < 0.01$) and VMN ($F_{1,40}$ =17.56, $p < 0.001$). Astrogliosis in 5xFAD mice was attenuated by DCI treatment, as shown by the specific genotype x treatment interaction in the ARC ($F_{1,40}$ =13.76, $p < 0.001$) and the VMN ($F_{1,40}$ =7.958, $p < 0.01$) (Fig. 5B, F). PVN analysis showed a sex x genotype interaction ($F_{1,40}$ =7.144, $p < 0.05$) and sex x treatment interaction ($F_{1,40}$ =5.587, $p < 0.05$), suggesting a specific effect of DCI on attenuation of GFAP immunofluorescence in the PVN of 5xFAD females (Fig. 5D). Specific comparison between groups showed significant differences between 5xFAD females and non-Tg females in the PVN ($p < 0.05$) and VMN ($p < 0.05$) and for 5xFAD males compared to non-Tg males in the VMN ($p < 0.05$) (Fig. 5D, F). DCI-treated 5xFAD females showed a significant reduction in GFAP signal when compared to 5xFAD females in the ARC ($p < 0.05$), PVN ($p < 0.01$) and VMN ($p < 0.01$) (Fig. 5B, D, F).

Analysis of the area covered by the GFAP signal showed a significant effect of genotype ($F_{1,40}$ =12.29, $p < 0.01$) and genotype x treatment interaction ($F_{1,40}$ =12.42, $p < 0.01$) only in the ARC (Fig. 5C). The area covered by the GFAP signal in the ARC differed significantly for both 5xFAD males and females compared to non-Tg mice ($p < 0.05$ for both), with a significant reduction in DCI-treated 5xFAD females ($p < 0.05$) (Fig. 5C). These results provide evidence that, despite the absence of Aβ deposition in the hypothalamus as determined by immunohistochemistry (Supplementary Figure 5), astrogliosis determined by GFAP immunofluorescence is present in several hypothalamic nuclei, including the ARC and VMN and also the PVN specifically in females, which is attenuated by DCI treatment.

We observed no significant differences in signal intensity for IBA1 staining, nor changes in the area covered by IBA1-positive cells (Supplementary Figures 4B-G). These results suggest that hypothalamic inflammation in 5xFAD mice is dependent on astroglial rather than microglial immunoreactivity.

3.5. Reduced plasma levels of insulin and insulin-related hormones are associated with hypothalamic inflammation

Since the hypothalamus is exposed to hormonal signals from the environment, we sought to determine whether changes in gene expression were related to an altered hormonal environment, or whether, on the contrary, the profile of pituitary hormones was affected by hypothalamic signaling (Fig. 6A, B). We performed correlation and hierarchical clustering analysis to assess the different associations between gene expression in the hypothalamus and plasma metabolites and hormones in both males and females.

In males, there was a defined cluster of insulin, GIP, cholesterol and TAGs, which were negatively associated with a cluster of hypothalamic inflammatory markers *Aif1, Il1b, Tnf*, but not *Gfap,* and conversely, were positively associated with the clustered hypothalamic neuropeptides *Npy, Agrp, Pomc, Ghrl, Ins2 and Cartpt* (Fig. 6A). These results suggest that peripheral signals showing a lack of nutrient availability in males were associated with low hypothalamic gene expression of neuropeptides regulating appetite and energy expenditure, and also with hypothalamic neuroinflammatory status.

Females, however, showed a defined cluster of insulin, GIP and GLP-1, with proximity to glucagon, resistin, and ghrelin, all negatively associated with neuroinflammation clustered in *Aif1, Tnf, Igf1, Gfap, Tlr4, and Il1b, but also Gnrh1* (Fig. 6B). The latter was significantly positively associated with FSH but did not reach statistical significance with LH, demonstrating its influence on increasing FSH production in 5xFAD females. Again, plasma levels of insulin, GIP, and GLP-1 were positively associated with *Npy, Agrp* and *Pomc*, and, in a separated cluster, with *Hcrt* and *Cartpt* (Fig. 6B). Specifically, BDNF was highly associated with hypothalamic *Igf1* and *Gfap,* suggesting that elevated

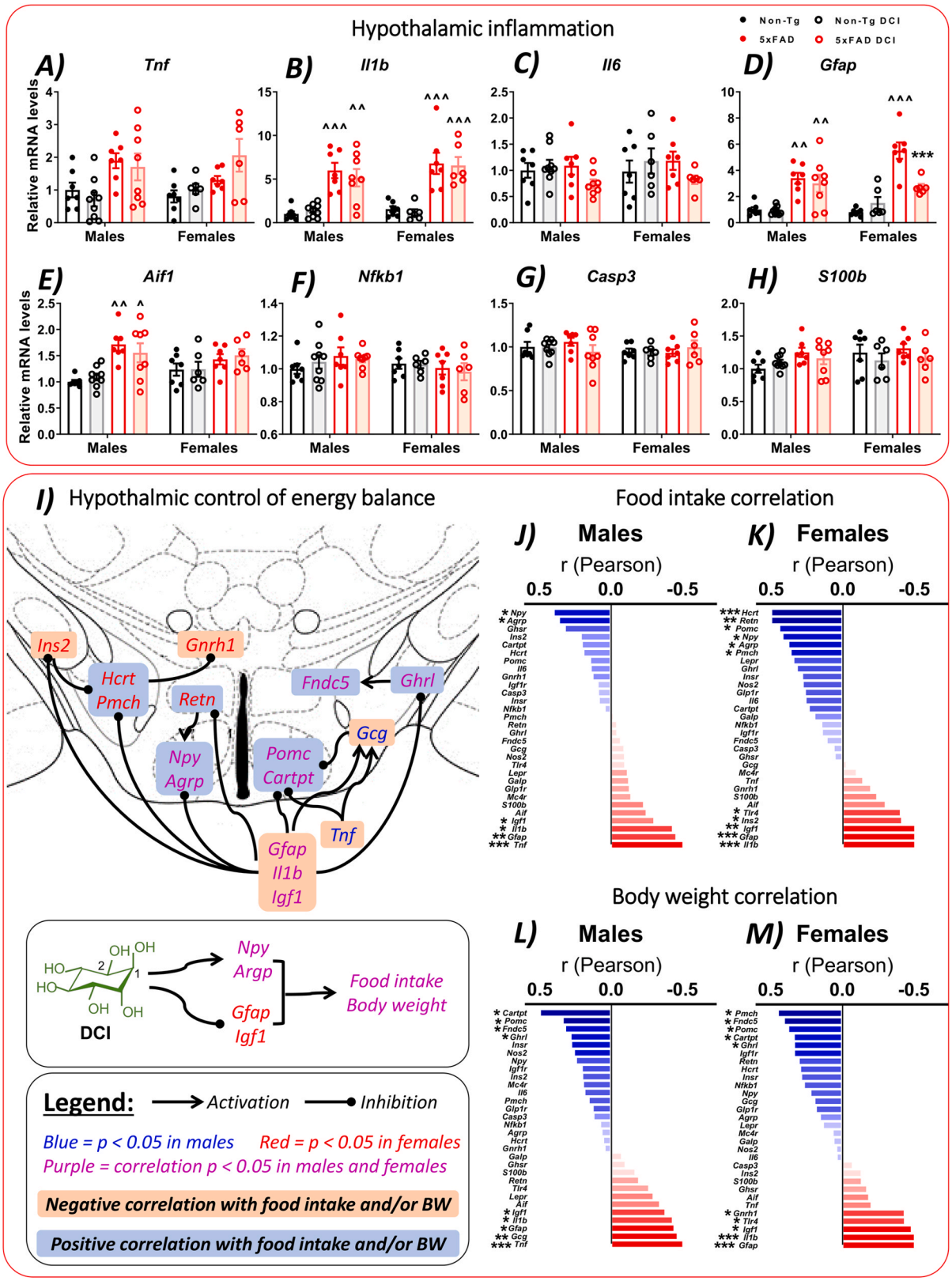

Fig. 4. Effect of DCI on hypothalamic inflammation and its correlation with food intake and body weight in male and female 5xFAD mice. A-H) Hypothalamic gene expression of the inflammatory markers tumoral necrosis factor (*Tnf*), interleukin 1b (*Il1b*), interleukin 6 (*Il6*), glial fibrillary acidic protein (*Gfap*), apoptosis inducible factor 1 (*Aif1*), nuclear factor-kappa-B p105 subunit (*Nfkb1*), caspase 3 (*Casp3*) and *s100b*. I) Schematic representation of dysregulated hypothalamic control of appetite and energy homeostasis based on gene expression analysis and associations and DCI effect on gene expression. J-M) Pearson correlations between expression of hypothalamic genes and either food intake or body weight in males and females. N = 6–9 per group. * = $p < 0.05$, ** = $p < 0.01$, *** = $p < 0.001$. Three-way ANOVA analysis (sex x genotype x treatment) with Tukey's post hoc test; significant differences between same-treatment non-Tg versus 5xFAD: * = $p < 0.05$, ** = $p < 0.01$, *** = $p < 0.001$; significant differences between same-genotype control versus DCI-treated: ^ = $p < 0.05$, ^^ = $p < 0.01$, ^^^ = $p < 0.001$.

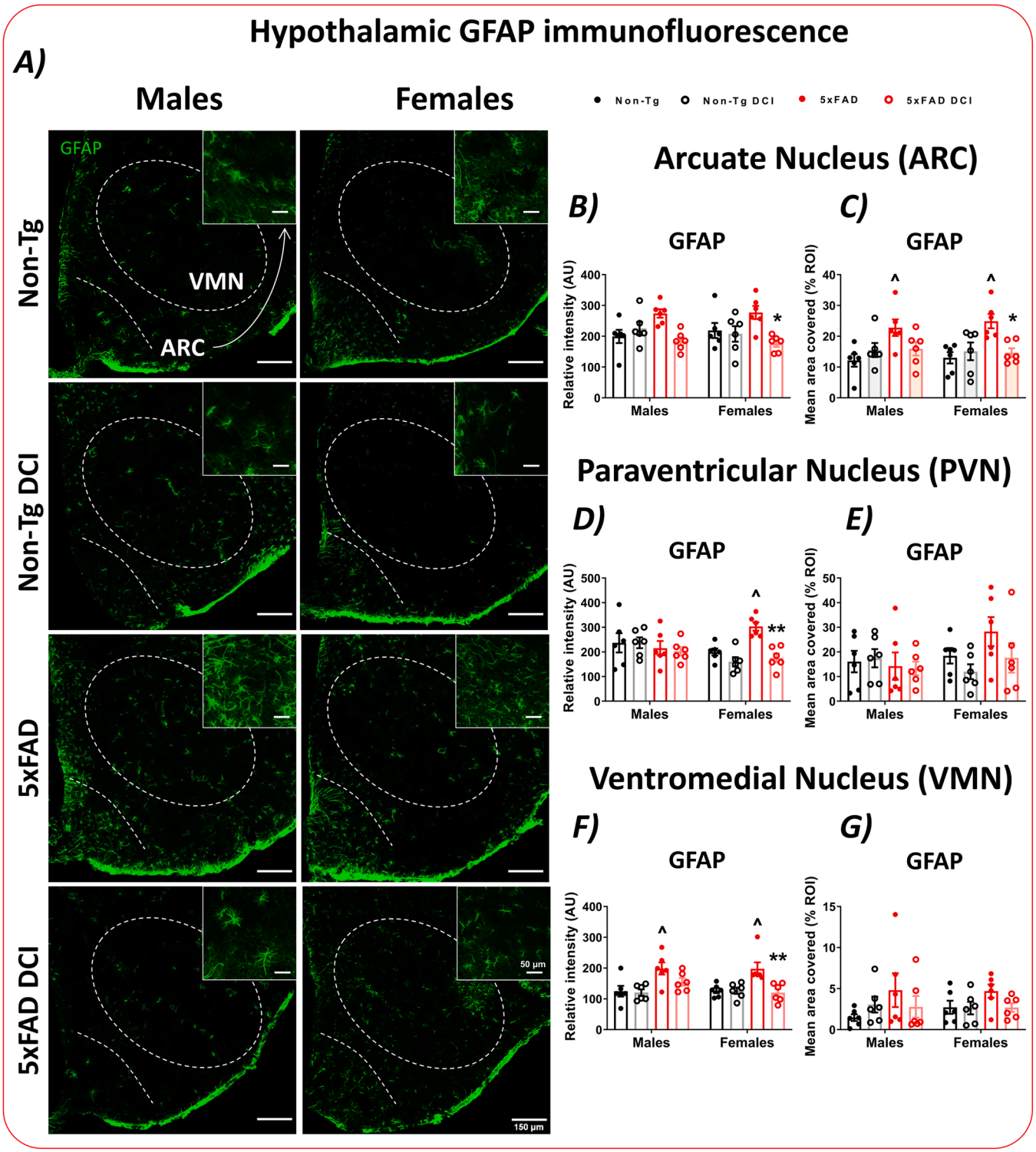

Fig. 5. Effect of DCI on hypothalamic astrogliosis as observed by GFAP immunofluorescence in a sex-dependent manner. A) Representative images at 10x (full image) and 20x (upper right subsection) of GFAP immunofluorescence in the hypothalamus of non-Tg and 5xFAD mice. Quantification of GFAP signal by relative intensity and area covered by GFAP-stained cells are depicted for specific hypothalamic nuclei: B-C) Arcuate nucleus (ARC); D-E) Paraventricular nucleus (PVN); F-G) Ventromedial nucleus (VMN). N = 6 per group with 3–4 replicates per brain. Three-way ANOVA analysis (sex x genotype x treatment) with Tukey's post hoc test; significant differences between same-treatment non-Tg versus 5xFAD: * = $p < 0.05$, ** = $p < 0.01$, *** = $p < 0.001$; significant differences between same-genotype control versus DCI-treated: ^ = $p < 0.05$, ^^ = $p < 0.01$, ^^^ = $p < 0.001$.

plasma levels of BDNF might be due to an inflammatory response rather than its usual trophic role (Fig. 6B).

3.6. DCI treatment attenuated the female-specific alteration of hepatic metabolism and fat accumulation in the liver of 5xFAD mice

The hypothalamus is connected to the liver and is able to regulate its

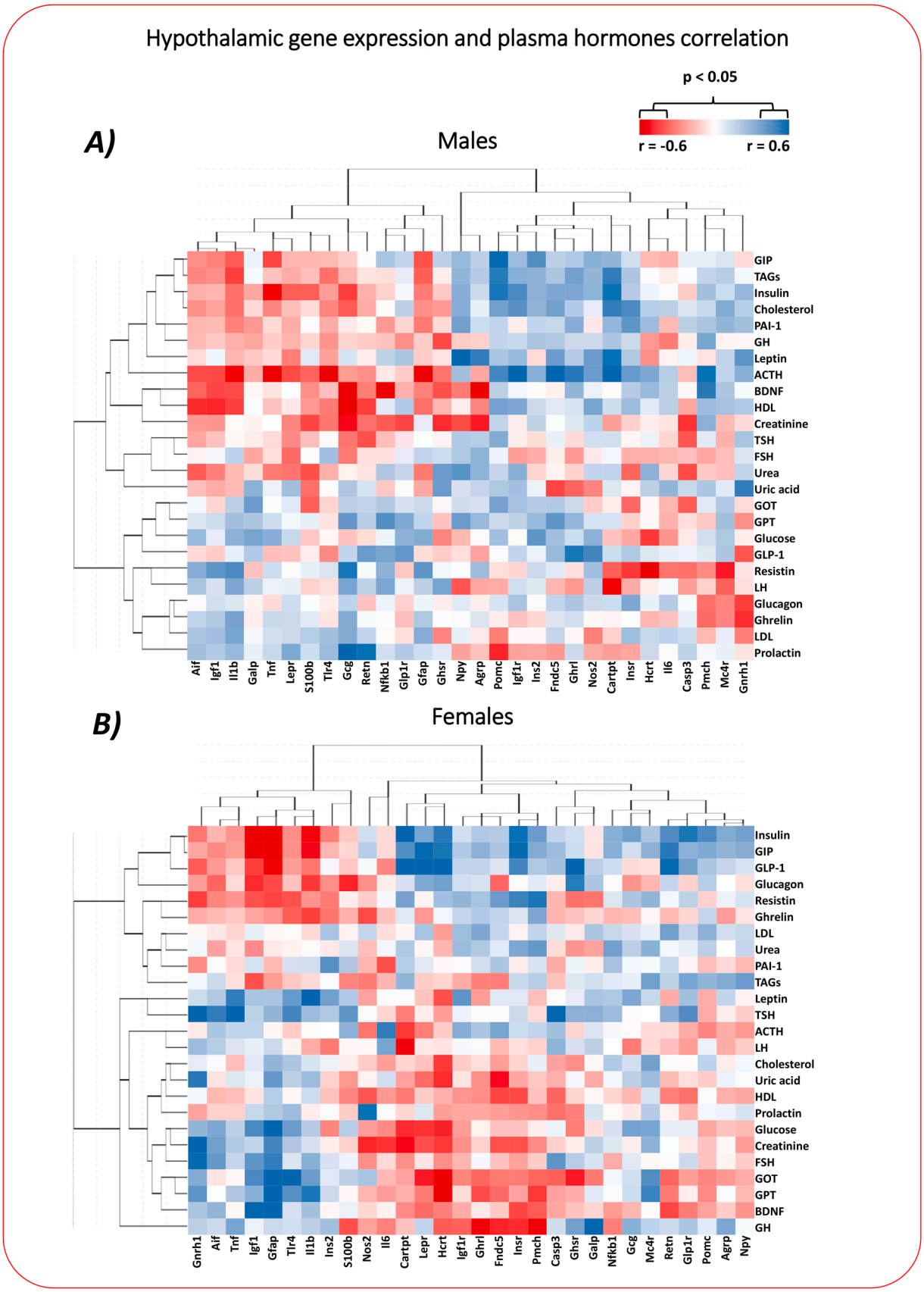

Fig. 6. Correlation analysis of hypothalamic gene expression and plasma hormones. Heatmap of Pearson correlation coefficients between plasma hormones and metabolites and hypothalamus gene expression of neuropeptides, endocrine and inflammatory markers showing hierarchical clustering of plasma insulin and insulin-related markers associated negatively to inflammatory gene expression and positively to neuropeptide gene expression in males and females.

metabolic state by neuroendocrine control via the hypothalamic-pituitary axis and sympathetic/parasympathetic efferent signaling [58]. In addition, hepatic metabolism is influenced and has an impact on plasma levels of hormones such as insulin, as well as cholesterol and TAGs [59], the levels of which were altered in 5xFAD mice, as previously observed. Moreover, there is an association between liver damage with AD prognostics and its major role in energy storage and the distribution and clearance of toxic substances such as Aβ [21–23]. Hence, we evaluated the status of the liver in 5xFAD mice.

Liver fat deposition was assessed in H-E sections and confirmed by total fatty acid extraction normalized per liver weight (Fig. 7A, B). Compared to males, females showed higher liver fat deposition (sex effect: $F_{1,51}$ =5.090, $p < 0.05$). This was mainly due to a higher liver fat content, specifically in 5xFAD females (sex x genotype interaction: $F_{1,51}$ =5.001, $p < 0.05$) (Fig. 7B). Overall, DCI treatment had a significant effect on reducing fat deposition regardless of sex (treatment effect: $F_{1,51}$ =3.839, $p < 0.05$), but also significantly reduced liver fat content in 5xFAD mice (genotype x treatment interaction: $F_{1,51}$ =6.541, $p < 0.05$) (Fig. 7B). Single comparisons showed that 5xFAD females had significantly higher liver fat levels than their non-Tg littermates ($p < 0.001$), whereas DCI-treated 5xFAD females did not differ significantly from non-Tg females, but had significantly lower fat deposition than untreated 5xFAD females ($p < 0.05$) (Fig. 7B). These results were confirmed by histological examination, showing both an increased accumulation of intracellular microvesicular fat and separation from extracellular macrovesicular fat (Fig. 7A).

Since female 5xFAD mice had lower body weight and presumably lower fat content, multiple linear regression analysis was performed to determine whether excess fat deposition in the liver was associated with or influenced by changes in hormones and metabolites, since alterations in insulin signaling may interfere with glucose and lipid metabolism in the liver, but also alter lipid storage in adipocytes and re-distribute free fatty acids (FFAs) to the liver, while pituitary hormones and metabolites may also influence liver metabolism. We found a significant negative association (Pearson r) between liver fatty acids and insulin, GLP-1 ($p < 0.01$ for all) (Fig. 7C, D), and also GIP ($p < 0.05$) (Supplementary Figure 3B). These associations show that low insulin signaling was somehow related to the hepatic accumulation of fatty acids. On the contrary, a positive association was found between liver fatty acids and FSH ($p < 0.001$) and also BDNF ($p < 0.05$) (Fig. 7E, F). Noteworthy, a positive association was also found between liver fatty acids and GPT ($p < 0.01$) and GOT ($p < 0.05$) levels (Supplementary Figures 6C, D), indicating that liver damage was preeminent due to ectopic fat storage in the liver.

The liver is an important organ responsible for receiving and storing circulating fatty acids, but also for the synthesis and secretion of TAGs and cholesterol. Fat accumulation in the liver and the development of fatty liver disease have been reported in cases of lipodystrophy and loss of subcutaneous fat [60]. Furthermore, the binding of Aβ peptides to hepatic lipid receptors, in addition to their presence in the liver, seems to trigger the inflammatory response [55,61]. Therefore, we analyzed the gene expression of metabolic pathways of fatty acid synthesis/degradation, lipid receptors, Krebs cycle, markers of oxidative stress, inflammation, cell death, as well as the endocannabinoid system, which is closely related to lipid metabolism in the liver (Fig. 7G, H). Volcano plot comparison between non-tg and 5xFAD females shows a significant overall increase in the expression of genes involved in lipid degradation, oxidative stress and inflammation, while there was a significant reduction of the main regulator of neoglucogenesis glucokinase (*Gck)*, and two enzymes involved in fatty acid de-saturation and TAGs secretion (*Srebf1* and *Dgat1*) (Fig. 7H). DCI treatment, however, reversed these changes in 5xFAD females, while decreasing the expression of leptin, IGF-1 and GLP-1 receptors (*Lepr, Igf1r and Glp1r*) and increasing estrogen receptor α (*Esr1*) (Fig. 7H).

DCI is known to be an insulin-sensitizing product. Since decreased plasma insulin in 5xFAD females is associated with liver fatty acid content and DCI treatment normalizes aberrant low insulin, we evaluated liver insulin signaling by western blotting (Fig. 7I-K). Specifically in females, DCI treatment significantly increased insulin receptor β (IRβ) phosphorylation (sex x treatment interaction: $F_{1,40}$ =6.541, $p < 0.05$) and IRS1 activity as determined by the ratio of inhibitory to activating phosphorylations at serine and tyrosine residues, respectively (sex x treatment interaction: $F_{1,40}$ =13.78, $p < 0.001$).

We performed a multiple linear regression analysis to determine the relationship between liver fatty acids, plasma insulin levels and dysregulated expression of genes involved in lipid metabolism and inflammation (Fig. 8A-C). We found strong positive associations between liver fatty acids and enzymes leading to acetyl-CoA formation, β-oxidation, lipid peroxidation and lipid receptors, whereas a significant negative association was found for fatty acid synthase (*Fasn*), TAG-formation (*Dgat1;* $p < 0.05$) and gluconeogenesis (*Gck*: $p < 0.05$) (Fig. 8B). These associations, however, were reversed when compared to plasma insulin, including the positive association with fatty acid de-saturases (*Fasn:* $p < 0.05$; *Scd1:* $p < 0.001$) and the negative association with an inflammatory marker (*Tnf:* $p < 0.05$) (Fig. 8C). Overall, insulin and insulin-related hormones showed similar associations with liver gene expression (Supplementary Figure 6E).

Our results presented here describe increased expression of liver lipid receptors, leading to increased internalization of FFAs and lipid lipoproteins, leading to fatty acid accumulation. These events, together with defective lipid de-saturation and secretion, promote fat accumulation in the liver, which in turn leads to an increased lipid β-oxidation response, oxidative stress and inflammatory response causing liver damage as observed by increased GOT and GPT levels (Fig. 8D). We propose that DCI treatment ameliorates liver metabolism by restoring insulin signaling and reducing lipid-mediated oxidative stress in 5xFAD females.

4. Discussion

There is a huge unmet demand for therapies targeting AD in its early and intermediate stages. One of the key elements in addressing the treatment and prevention of AD is the lack of objective diagnostic and follow-up tools. Epidemiological studies reveal that weight loss and obesity [61], altered metabolic parameters such as hyperglycemia, hypo- and hyperinsulinemia, hypoleptinemia, liver damage and changes in microbiota are positively correlated with the development of AD in humans [14,15,62]. Currently, there are preclinical pharmacological approaches and recent clinical trials based on the use of drugs normally studied in diabetes, such as metformin or intranasal insulin itself, in AD [63–65]. Another proposed approach is the use of nutraceuticals, natural substances included in the diet such as DCI, which is an agent known to act as a non-canonical messenger and sensitize tissues to insulin actions. DCI and its 3-O-methyl-derivative, D-Pinitol, have been shown to be effective for the treatment of diabetes, and fatty liver, in addition to showing promising in vitro results against Aβ deposition, γ-secretase inhibitory activity, and decreased Tau hyperphosphorylation in rodents [66]. In our study, we aimed to demonstrate the therapeutic efficacy of DCI in the 5xFAD model, an animal model of AD that exhibits early memory deficits and cognitive impairment and a phenotype of metabolic dysregulation which is expressed differently in males and females, highlighting deficits in body weight, plasma insulin and fatty acid levels [10,67–69].

Weight loss is known to be observed in certain cases of AD in prodromal states, while BMI is also a marker of cognitive impairment for AD, and both appear to be related to alterations in eating and sleeping patterns [70–73]. This generalized weight loss was consistent with a lower cumulative food intake in both 5xFAD males and females. This trait had previously been observed in 5xFAD animals [10,67–69,74]. Although previous studies suggest that weight loss in 5xFAD mice could be a consequence of hyperactivity [75], as occurs in other transgenic models of AD such as the Tg4510 and 3xTg mice [16,76,77], we found

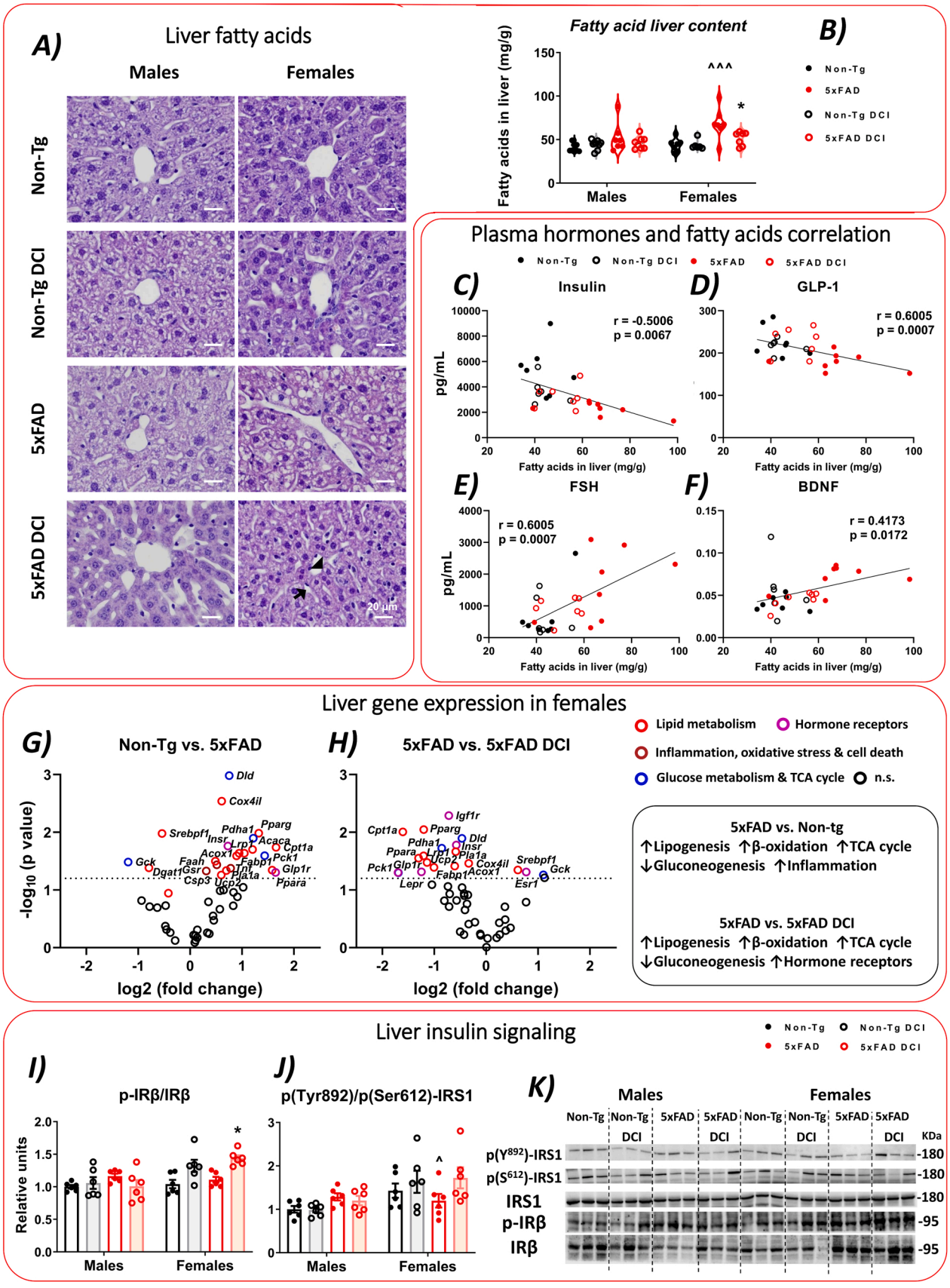

(caption on next page)

Fig. 7. Effect of DCI on fatty acid accumulation and expression of lipid oxidation pathways and insulin signaling in the liver of male and female 5xFAD mice. A) Staining of liver sections with hematoxylin and eosin (H&E), with microvascular (arrowhead) and macrovascular (arrow) deposits of fat pointed with black arrows in image placed down right. B) Liver fat content normalized per liver weight. C-D) Pearson correlation of plasma hormones with liver fat content in females. G-H) Volcano plots of liver gene expression from non-Tg versus 5xFAD females and 5xFAD females versus DCI-treated females, with color scheme of gene-related pathways showing significant differences. Threshold line indicates $p < 0.05$. I-J) Protein expression regarding activity of insulin receptor β (IRβ) as determined by tyrosine phosphorylation and insulin receptor substrate 1 (IRS1) activity determined by the ratio of activating (Tyr) and inhibitory (Ser) phosphorylation. K) Representative Western blot images (see also Figs. S4 and S5). N = 6–9 per group. Three-way ANOVA analysis (sex x genotype x treatment) with Tukey's post hoc test; significant differences between same-treatment non-Tg versus 5xFAD: * = $p < 0.05$, ** = $p < 0.01$, *** = $p < 0.001$; significant differences between same-genotype control versus DCI-treated: ^ = $p < 0.05$, ^^ = $p < 0.01$, ^^^ = $p < 0.001$.

that 5xFAD animals exhibited lower metabolic rate, which is probably a sum of an adaptation to lower energy availability and loss of mobility related to neurodegeneration, as previously observed in 5xFAD females at an earlier age than in this study [69,78]. DCI treatment, which increases food intake in 5xFAD mice, only partially restores energy expenditure in these animals, specifically in females. This phenomenon leads us to think that motor problems and decreased activity have a major impact on the lower rate of energy expenditure. The mechanism by which DCI partially restores appetite in 5xFAD mice will be discussed later in this section, as it is likely to involve hypothalamic inflammation and neuroendocrine signaling.

The fact that obesity and cardiovascular problems are predictive of a higher incidence of AD has led to multiple longitudinal studies relating plasma levels of TAGs, cholesterol, or lipid proteins to the onset of symptoms or prevalence in AD. Elevated cholesterol or LDL and low HDL levels have been shown to contribute to the risk for AD, due to changes in the membrane structure of neurons and the accumulation and processing of amyloid fragments [79,80]. However, the generalized results remain controversial, as other studies show that lipid therapy increasing LDL levels and decreasing HDL levels in AD patients promotes better scores on cognitive tests [81]. Regarding animal studies, high-throughput techniques have depicted an altered lipid distribution in the brain of 5xFAD mice along with Aβ pathology [82,83]. This led us to study the impact of DCI on the plasma lipid profile of 5xFAD mice since DCI treatment in patients with metabolic syndrome shows its efficacy in reducing elevated levels of TAGs and LDL [84]. We found overall low levels of TAGs and cholesterol in 5xFAD mice, with these changes being more evident in 5xFAD males. These results at 10–12 months of age are consistent with a previous study showing low plasma levels of TAGs and total cholesterol in 5xFAD males and females at 12 months of age. While this study also showed decreased HDL and LDL in males, we found no significant differences in 5xFAD mice [75]. The decrease in TAG and cholesterol levels in 5xFAD animals may be a consequence of lower fat content in adipose tissue, as previously described [67]. Another possible cause is a shift from glucose to lipid utilization as an energy source, in agreement with the decrease in RQ observed in 5xFAD mice, since lower RQ measurements correlate with higher O_2 consumption in lipid β-oxidation. DCI treatment slightly normalizes plasma TAG levels in 5xFAD to equal those in non-Tg mice, while conversely increasing plasma LDL in non-Tg mice. The DCI-mediated increase in TAG levels may be due to either body weight gain and increased fat deposition in adipose tissue or normalization of hepatic function in 5xFAD mice, as the liver is a major source of plasma TAGs.

Our AD model presented a generalized age-dependent defect of endocrine signaling, especially in hormones related to insulin signaling. Follow-up studies in humans have highlighted the predictive value of fasting plasma insulin levels in AD, showing that excessively low basal insulin levels were greater predictors of risk for the subsequent development of dementia and AD compared to high insulin levels, independently of preclinical development of type 2 diabetes [14,85]. This outlines a U-shaped association between fasting plasma insulin levels and the risk of developing AD. We have previously described that 5xFAD animals already have low plasma insulin levels at 6 months of age [10]. Other authors have observed in the 3xTg model a progressive loss of pancreatic β-cell mass with age and low glucose tolerance [17,87]. In addition to insulin, an age-dependent decrease in intestinal hormone release has also been previously described in 3xTg animals. The combination of these events may lead to a decrease in insulin and its signaling in 5xFAD animals. In our study, DCI was able to partially reverse the loss of GIP, GLP-1 and insulin release in 5xFAD animals. Previous studies have shown DCI and its analog, D-Pinitol, can increase basal insulin secretion, and are able to prevent pancreatic mass loss by reducing oxidative stress in streptozotocin-injected rats (type 1 diabetes model), as well as restore insulin immunoreactivity in KK-A^y mice (type 2 diabetes model) [88–90]. The accumulation of Aβ plaques in the gastrointestinal tract could be affecting the functionality of the K (GIP-secreting) or L (GLP-1-secreting) cells, similarly to what has been observed by immunofluorescence techniques in the pancreas of other animal models of AD [17,87]. Another possible cause may rely on increased oxidative stress and inflammatory response to the presence of amyloid peptides or systemic inflammation. Since it is beyond the scope of this article, we have not examined the tissue integrity of the intestinal tract of 5xFAD mice. However, this possibility should not be ruled out, since expression of transgenic human APP is detected in the duodenum and jejunum of 5xFAD mice [91]. On the other hand, 5xFAD animals also present an altered microbiota at advanced ages [91]. Secretion of GLP-1 and GIP correlates with the over- or under-representation of certain bacterial families, which are associated with inflammatory processes [92]. Supplementation with D-Pinitol enriched diet modulates the altered gut microbiota in type 2 diabetic rats, restoring the abundance of bacteria associated with glycemic control [93]. Hence, DCI treatment could infer the microbiome of 5xFAD mice in a mechanism involving deficient production of GIP and GLP-1.

When pituitary hormones were analyzed, especially plasma ACTH levels decreased in 5xFAD males, while plasma BDNF and FSH increased in 5xFAD females. These changes were reversed with DCI treatment. Elevated plasma FSH levels may be due to loss of fertility in 5xFAD females, as increased hormonal stimulation is necessary for the maturation of ovules [94]. Likewise, it has been observed in postmenopausal women that high FSH levels are negatively associated with low basal insulin levels [95]. Interestingly, DCI treatment is currently prescribed in women with fertility disorders and polycystic ovary syndrome, and DCI is able to restore altered plasma levels of FSH and LH, as well as sex steroid production. Because the wide neuroprotective and metabolism-modulating actions of sex steroids might account for the current beneficial actions of DCI, future studies must clarify whether sex steroid homeostasis is disrupted in 5XFAD mice and restored by DCI supplementation. Regarding ACTH, this hormone is a by-product of POMC cleavage. We propose that the low plasma ACTH levels in 5xFAD males are associated with a generalized decrease in *Pomc* expression, as observed in the hypothalamus. Finally, the elevation of BDNF in 5xFAD females is paradigmatic, as conflicting results have been found regarding plasma BDNF concentration in cognitive impairment, but elevated BDNF levels have been previously observed in patients with moderate AD, probably associated with a stress reaction and inflammation [96]. Dimension reduction analysis with plasma analytes differentiated 5xFAD mice from non-Tg in a sex-specific manner. Discrimination in males resided in cholesterol levels, TAGs, and ACTH, whereas females differed mainly in components related to liver damage, insulin homeostasis and FSH. DCI-treated 5xFAD mice were distributed similarly to non-Tg littermates, suggesting its effectiveness in restoring

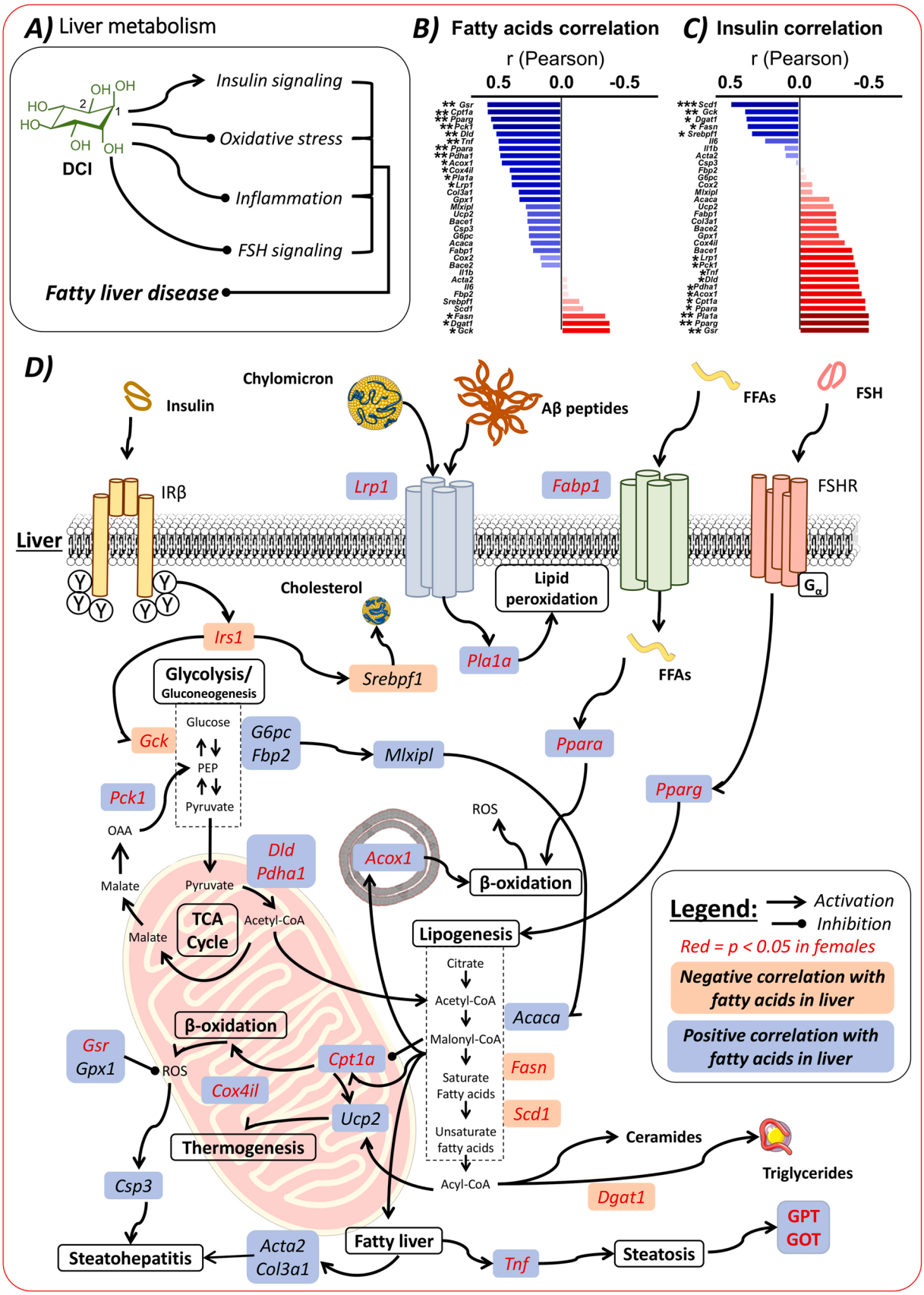

Fig. 8. Schematic representation of dysregulated liver metabolism in 5xFAD females and effect of DCI on inflammation, oxidative stress and endocrine signaling. A) Scheme of dysregulated liver metabolic pathways towards fatty acid oxidation based on gene expression, plasma hormone levels and protein activity measurements. B-C) Pearson correlations between expression of liver genes and either liver fat content or plasma insulin in females. D) DCI effect on attenuating imbalance of liver metabolism. N = 6–9 per group. * = $p < 0.05$, ** = $p < 0.01$, *** = $p < 0.001$.

hormonal deficiencies, at least partially in the AD genotype. This analysis provides us with a useful tool for the AD prognosis based on prodromal blood tests, and highlights the need to tailor these prognostically oriented blood tests to the sex of the patient.

In previous experiments by our group, we had already observed a loss of hypothalamic insulin and leptin signaling in male and female 5xFAD animals, although the expression of the main neuropeptides controlling food intake in the ARC and PVN, *Npy*, *Agrp*, *Pomc* and *Cartpt* were not significantly affected at 6 months of age [10]. Other authors have associated reduced food intake in 5xFAD mice with neurodegenerative and motor problems leading to difficulty in chewing [51]. In the present study, we observed a marked loss of expression of *Pomc* and *Cartpt* in 5xFAD mice upon reaching 10 months of age, which seems to reflect the lack of hormonal insulin and leptin signaling in the hypothalamus [13,16]. Although the decreased expression of orexigenic neuropeptides *Npy*, *Agrp*, and *Pmch* in 5xFAD mice is not as pronounced, this state reflects the loss of the ability to control energy intake and expenditure in 5xFAD animals at an advanced age. This is consistent with studies in other mouse models of AD describing the loss of *Npy* expression due to the presence of Aβ fragments [4]. DCI is known to increase hypothalamic expression of *Npy* and *Agrp* in fasted mice, while the opposite is observed in diet-induced obese mice [97]. Our study shows that DCI can increase the expression of *Npy* and *Agrp*, which is reflected in increased food intake, preventing progressive weight loss in 5xFAD mice. The specific effect of DCI on other neuropeptides such as *Galp* and *Retn* in 5xFAD females is intriguing, although both are known to promote feeding through induction of *Npy/Agrp* [98,99].

In our study, we found that most of the changes in the expression of neuropeptides in the hypothalamus were related to the expression of inflammatory cytokines, more specifically *Il1b*, *Tnf* or *Gfap*, which lead to decreased food intake and weight loss. It has been previously reported that increased *Il1b* and *Tnf* levels in the hypothalamus can promote a state of hypophagia [100,101] or a decrease in energy expenditure and insulin sensitivity [102]. Although DCI is known to exert an anti-inflammatory effect under certain conditions, we did not observe changes in pro-inflammatory cytokines expression in 5xFAD mice. Intriguingly, we observed a decline in *Il6* below normal levels in DCI-treated 5xFAD mice. Hypothalamic *Il6* expression reduces *Pomc* and *Npy* expression [103], but we only observed a significant negative association between *Il6* and *Agrp* in both males and females. Hence, the effect of DCI on *Il6* expression and its possible contribution to hypothalamic regulation of energy homeostasis remains undisclosed.

We found a sex-specific effect for DCI on *Gfap* and *Igf1* expression in 5xFAD females. Hypothalamic expression of *Igf1* rises in parallel to that of *Gfap*. Although the autocrine activity of *Igf1* in the brain appears to exert neuroprotective effects on glia [104], cytokine production is known to trigger its expression, so the observed *Igf1* expression may be a consequence of astrocyte activation [105]. The fact that *Gfap* was negatively associated with the expression of orexigenic and anorexigenic neuropeptides suggests that astroglial activation significantly interferes with hypothalamic neuronal activity. Moreover, immunofluorescence analysis revealed that the GFAP signal was preeminently associated with the ARC and VMN, major regulators of food intake, and also the PVN in 5xFAD females. However, there were no changes in IBA1 immunoreactivity in the aforementioned hypothalamic areas. In addition, DCI treatment also normalized GFAP immunofluorescence in the mentioned hypothalamic areas. Therefore, these results suggest that hypothalamic dysfunction in 5xFAD mice is dependent on astrogliosis rather than microgliosis. *Gfap* activation in the hypothalamus of 5xFAD animals is likely triggered by the presence of Aβ deposits. Although neuroanatomy techniques did not discern an accountable amount of Aβ plaques in the hypothalamus of 5xFAD mice, the occurrence of Aβ oligomers, which are known to promote glial and astrocytic reactivity, cannot be ruled out. Hence, future studies should investigate the possible presence of Aβ oligomers concerning hypothalamic inflammation in 5xFAD mice. *In vitro* assays have shown that DCI potentiates insulin-mediated inhibition of diffusible Aβ-derived ligands, which are neurotoxic and induce damage at synapses in neurons [3]. We have found that low plasma insulin and associated metabolites are related to increased hypothalamic inflammation and neuroendocrine signaling in a triangle-like event leading to impaired appetite and weight loss. Therefore, we represent a model in which the DCI promotes food intake and regulates body weight in 5xFAD mice by promoting the expression of orexigenic neuropeptides and normalizing the secretion of hormones responsible for maintaining energy homeostasis.

To have a more complete picture of metabolic dysfunctions associated with the expression of the 5xFAD mutations, we decided to evaluate the metabolic and inflammatory status of the liver, in agreement with previous research associating liver pathologies with the severity of AD. Elevated plasma levels of GPT and GPT were found to be associated with the diagnosis of AD (56) in a mechanism that may involve systemic clearance of diffusible Aβ oligomers in the liver. Moreover, Aβ aggregates may be taken up and internalized by the liver through lipid receptors such as LRP1 [21]. The hepatoprotective capacity of DCI has been previously investigated, outlining its efficacy in alleviating oxidative stress and hepatic inflammatory response, as well as reducing the lipid accumulation that subsequently leads to hepatic steatosis [33,106,107].

The fatty liver observed in 5xFAD females arouses curiosity, as this AD model presents lower storage of white adipose tissue [67]. The accumulation of lipids in the liver is progressive and follows the loss of adipose tissue, as has been previously described [67]. It has been previously reported in other animal models of AD, such as the 3xTg, that, despite presenting a lower body weight phenotype, the liver shows a higher fat content and an increased inflammatory response [55]. In our case, this effect was specifically observed in 5xFAD females, so we decided to study hepatic metabolism in this sex. Interestingly, in our model, the accumulation of fatty acids was associated with a decrease in plasma insulin levels, but in turn with an increase in plasma FSH and BDNF. This trend resembles a model of lipodystrophy, in which deficiency of insulin signaling or insulin-responsive hormone-sensitive lipase (HSL) activity in adipose tissue results in lower plasma TAG content, but increased accumulation of fatty acids in the liver [108]. However, our model showed an activated response of increased mitochondrial β-oxidation and peroxidation, which was not able to alleviate lipid accumulation. In addition, gluconeogenesis was decreased, and the Krebs cycle pathway resulted in the generation of acetyl-CoA as a substrate for fatty acid oxidation, while the fatty acid de-saturation pathway was decreased.

The liver is known to express the FSH receptor (FSHR) [109], while elevated levels of FSH promote lipid biosynthesis through the PPAR-γ pathway [110]. An inverse relationship between levels of FSH in plasma and the prevalence of fatty liver has been demonstrated [111], being a possible partial explanation for a more pronounced fatty liver phenotype in 5xFAD females. The 5xFAD mouse liver expresses human APP protein (Supplementary Fig 6A), and the presence of hepatic amyloidosis in 5xFAD animals has been described previously [112]. The specific expression of amyloid protein in the liver of mice results in steatosis at a similar age (12 months), in addition to an increase in GPT levels [113]. This indicates that amyloid protein accumulation directly interferes with the hepatic metabolism in the 5xFAD model, aggravating the previously observed metabolic defects. Although DCI is able to prevent the formation of diffusible Aβ oligomers in neurons in vitro, there are still no studies on its efficacy in vivo in the periphery. Hence, future studies on this topic could describe a potential mechanism to prevent systemic inflammation and toxicity resulting from AD. Since the decrease in insulin signaling was associated with the appearance of fatty liver in 5xFAD females, similar to what occurs in mouse models of type 1 diabetes [114], we observed that DCI is able to restore plasma insulin levels and the activity of the insulin receptor (IR) and its second messenger (IRS1) in the liver, which was associated with a decrease in hepatic fatty acid accumulation. DCI is also able to reduce the inflammatory response

and hepatic oxidative stress, as observed by decreased levels of *Tnf*, GOT and GPT. Overall, DCI treatment is able to partially restore metabolic flux in the liver of 5xFAD females.

5. Limitations of the study

Most cases of AD are sporadic in origin. For this reason, the vast majority of studies on AD, including body weight and hormonal disorders, are described in patients with sporadic AD [5–7]. Animal models of AD, such as the 5xFAD mouse, reproduce AD events by expressing mutant forms of the human APP and PSEN1 proteins, described in familial AD. These animal models attempt to mirror as closely as possible the human pathology of AD, even though its origin is not sporadic.

In our study, the animals were separated to control weekly food consumption and to ensure that all animals drank a similar amount of the DCI compound dissolved in the water. We tried to control the possible impact of isolating the mice in all experimental groups under the most appropriate conditions possible.

It has been previously described that 5xFAD mice show lower fat storage in the white adipose tissue [67]. This fact may lead us to hypothesize that the changes in the RQ of the 5xFAD mice are due to the utilization of fat as an energy source, and the effect of the DCI on the normalization of the RQ is due to the weight and fat gain in 5xFAD mice (or the avoidance of progressive loss of fat in 5xFAD mice). This is supported by previous data showing the efficacy of DCI and DCI-analogues such as myo-inositol in promoting insulin signaling, lipogenesis, and lipid accumulation in mature adipocytes [31,115]. We have preliminary data by bioimpedance spectroscopy analysis suggesting an increase in fat tissue in 5xFAD animals treated with DCI. However, the number of animals on which we performed the analysis was small, so we can only suggest, but not strongly confirm, this fact. We acknowledge the importance of future studies to confirm the changes in white adipose tissue in DCI-treated mice and their possible implications for the metabolic and hormonal disorders described.

6. Conclusions

In summary, we have analyzed the efficacy of dietary supplementation with DCI, an insulin response enhancer, in the 5xFAD model of AD, which presents metabolic disorders that lead to weight loss and sex-specific hormonal alterations. We have found that the inflammatory process in the hypothalamus and the loss of insulin signaling negatively affect appetite, leading to progressive weight loss. The ability of DCI to reduce inflammation and restore hormonal signaling contributes in part to preventing the metabolic decline in 5xFAD animals. Furthermore, we found the appearance of specific signs of fatty liver in 5xFAD females, in contrast to their low body weight, which was associated with a dysregulation of endocrine signaling in this model. DCI treatment can reverse this phenotype of energy dysregulation. This study opens up a range of possibilities regarding the potential efficacy of insulin-sensitizing agents, such as DCI, in the development of metabolic disorders that may lead to aggravation of AD. Future studies should focus on analyzing the involvement of sex steroids, and amyloid pathology in the gut and liver, in addition to analyzing the impact of the microbiota on the decrease in the secretion of hormones from the intestinal tract in order to provide less invasive early diagnostic tools and targets for treatment.

Funding

This research was funded by the European Regional Development Funds-European Union (ERDF-EU) and Fatzheimer project EULAC-HEALTH H2020, grant number EU-LACH16/T010131; Ministerio de Economía, Industria y Competitividad, Gobierno de España, grant number RTC-2016-4983-1; EU-ERDF and Instituto de Salud Carlos III (ISCIII), grant numbers PI19/01577 and PI19/00343; Ministerio de Sanidad, Delegación de Gobierno para el Plan Nacional sobre Drogas, grant numbers 2019/040 and 2020/048; Consejería de Transformación Económica, Industria, Conocimiento y Universidades, Junta de Andalucía, grant number P18-TP-5194, INSERM (Institut National de la Santé et de la Recherche Médicale), Nouvelle Aquitaine Region and ANR (grant numbers ANR-18-CE14-0029 MitObesity, Labex BRAIN ANR-10-LABX-43, ANR-10-EQX-008-1 OPTOPATH, ANR-17-CE14-0007 BABrain, ANR-21-CE14-0018-01_StriaPOM to D.C.). A.J.L.-G. (IFI18/00042) holds an "iPFIS" predoctoral contract from the National System of Health, EU-ERDF-ISCIII. B.P.S (IFI21/00024) holds an "iPFIS" predoctoral contract from the National System of Health, EU-ERDF-ISCIII. P.R. (CP19/00068) holds a ''Miguel Servet I" research contract from the National System of Health, EU-ERDF-ISCIII. D.M-V. (FI20/00227) holds a "PFIS" pre-doctoral contract from the National System of Health, EU-ERDF-ISCIII. The microscopy for IBA1 and GFAP immunofluorescence was done in the Bordeaux Imaging Center, a service unit of the CNRS-INSERM and Bordeaux University, member of the national infrastructure France BioImaging supported by the LabEX BRAIN and ANR-10-INBS-04. Funding for open access charge: Universidad de Málaga / CBUA.

CRediT authorship contribution statement

Antonio J. López-Gambero: Conceptualization, Methodology, Validation, Formal analysis, Investigation, Resources, Data curation, Writing – original draft, Writing – review & editing. **Beatriz Pacheco-Sánchez:** Methodology. **Cristina Rosell-Valle:** Methodology, Formal analysis. **Dina Medina-Vera:** Methodology, Formal analysis. **Juan Antonio Navarro:** Methodology. **María del Mar Fernández-Arjona:** Methodology. **Marialuisa de Ceglia:** Formal analysis. **Carlos Sanjuan:** Validation. **Vincent Simon:** Methodology. **Daniela Cota:** Validation, Resources, Writing – review & editing, Supervision, Project administration, Funding acquisition. **Patricia Rivera:** Validation, Resources, Writing – review & editing, Supervision, Project administration, Funding acquisition. **Fernando Rodríguez de Fonseca:** Conceptualization, Validation, Investigation, Writing – review & editing, Supervision, Project administration, Funding acquisition. **Juan Suárez:** Conceptualization, Validation, Investigation, Resources, Data curation, Writing – original draft, Writing – review & editing, Supervision, Project administration, Funding acquisition..

Conflict of interest statement

C.S. declares he receives a salary from and has shares in the Euronutra S.L. company. The remaining authors declare that they have no known competing financial interests or personal relationships that could have appeared to influence the work reported in this paper. The funders had no role in the design of the study; in the collection, analyses, or interpretation of data; in the writing of the manuscript; or in the decision to publish the results.

Appendix A. Supporting information

Supplementary data associated with this article can be found in the online version at doi:10.1016/j.biopha.2022.112994.

References

[1] 2020 Alzheimer's disease facts and figures, Alzheimers Dement (2020).
[2] A.J. López-Gambero, C. Sanjuan, P.J. Serrano-Castro, J. Suárez, F. Rodríguez de Fonseca, The biomedical uses of inositols: a nutraceutical approach to metabolic dysfunction in aging and neurodegenerative diseases, Biomedicines 8 (9) (2020) 295.
[3] J. Pitt, M. Thorner, D. Brautigan, J. Larner, W.L. Klein, Protection against the synaptic targeting and toxicity of Alzheimer's-associated Aβ oligomers by insulin mimetic chiro-inositols, FASEB J. 27 (1) (2013) 199–207.
[4] M.J. McGuire, M. Ishii, Leptin dysfunction and Alzheimer's disease: evidence from cellular, animal, and human studies, Cell. Mol. Neurobiol. 36 (2) (2016) 203–217.

[5] D.K. Johnson, C.H. Wilkins, J.C. Morris, Accelerated weight loss may precede diagnosis in Alzheimer disease, Arch. Neurol. 63 (9) (2006) 1312–1317.

[6] T. Möllers, H. Stocker, L. Perna, A. Nabers, D. Rujescu, A.M. Hartmann, B. Holleczek, B. Schöttker, K. Gerwert, H. Brenner, Aβ misfolding in blood plasma is inversely associated with body mass index even in middle adulthood, Alzheimers Res. Ther. 13 (1) (2021) 145.

[7] E.D. Vidoni, R.A. Townley, R.A. Honea, J.M. Burns, Alzheimer disease biomarkers are associated with body mass index, Neurology 77 (21) (2011) 1913–1920.

[8] S.J. Baloyannis, I. Mavroudis, D. Mitilineos, I.S. Baloyannis, V.G. Costa, The hypothalamus in Alzheimer's disease: a Golgi and electron microscope study, Am. J. Alzheimers Dis. Other Demen 30 (5) (2015) 478–487.

[9] D.J. Callen, S.E. Black, F. Gao, C.B. Caldwell, J.P. Szalai, Beyond the hippocampus: MRI volumetry confirms widespread limbic atrophy in AD, Neurology 57 (9) (2001) 1669–1674.

[10] A.J. López-Gambero, C. Rosell-Valle, D. Medina-Vera, J.A. Navarro, A. Vargas, P. Rivera, C. Sanjuan, F. Rodríguez de Fonseca, J. Suárez, A Negative Energy Balance Is Associated with Metabolic Dysfunctions in the Hypothalamus of a Humanized Preclinical Model of Alzheimer's Disease, the 5XFAD Mouse, Int. J. Mol. Sci. 22 (10) (2021) 5365.

[11] K. Do, B.T. Laing, T. Landry, W. Bunner, N. Mersaud, T. Matsubara, P. Li, Y. Yuan, Q. Lu, H. Huang, The effects of exercise on hypothalamic neurodegeneration of Alzheimer's disease mouse model, PloS One 13 (1) (2018) e0190205-e0190205.

[12] M. Ishii, G. Wang, G. Racchumi, J.P. Dyke, C. Iadecola, Transgenic mice overexpressing amyloid precursor protein exhibit early metabolic deficits and a pathologically low leptin state associated with hypothalamic dysfunction in arcuate neuropeptide Y neurons, J. Neurosci. 34 (27) (2014) 9096–9106.

[13] M. Ishii, A.J. Hiller, L. Pham, M.J. McGuire, C. Iadecola, G. Wang, Amyloid-beta modulates low-threshold activated voltage-Gated L-type calcium channels of arcuate neuropeptide Y neurons leading to calcium dysregulation and hypothalamic dysfunction, J. Neurosci. 39 (44) (2019) 8816–8825.

[14] K. Mehlig, L. Lapidus, D.S. Thelle, M. Waern, H. Zetterberg, C. Björkelund, I. Skoog, L. Lissner, Low fasting serum insulin and dementia in nondiabetic women followed for 34 years, Neurology 91 (5) (2018) e427–e435.

[15] E. Rönnemaa, B. Zethelius, J. Sundelöf, J. Sundström, M. Degerman-Gunnarsson, C. Berne, L. Lannfelt, L. Kilander, Impaired insulin secretion increases the risk of Alzheimer disease, Neurology 71 (14) (2008) 1065–1071.

[16] M. Ishii, G. Wang, G. Racchumi, J.P. Dyke, C. Iadecola, Transgenic mice overexpressing amyloid precursor protein exhibit early metabolic deficits and a pathologically low leptin state associated with hypothalamic dysfunction in arcuate neuropeptide Y neurons, J. Neurosci. Off. J. Soc. Neurosci. 34 (27) (2014) 9096–9106.

[17] C.M. Griffith, L.N. Macklin, Y. Cai, A.A. Sharp, X.X. Yan, L.P. Reagan, A. D. Strader, G.M. Rose, P.R. Patrylo, Impaired glucose tolerance and reduced plasma insulin precede decreased AKT phosphorylation and GLUT3 translocation in the hippocampus of Old 3xTg-AD mice, J. Alzheimers Dis. 68 (2) (2019) 809–837.

[18] C. Sha, W. Hu, C. Iadecola, M. Ishii, Circulating leptin in the preclinical stage of Alzheimer's disease (4065), Neurology 94 (15 Supplement) (2020) 4065.

[19] X. Cao, M. Zhu, Y. He, W. Chu, Y. Du, H. Du, Increased serum acylated ghrelin levels in patients with mild cognitive impairment, J. Alzheimers Dis. 61 (2) (2018) 545–552.

[20] R.A. Short, R.L. Bowen, P.C. O'Brien, N.R. Graff-Radford, Elevated gonadotropin levels in patients with Alzheimer disease, Mayo Clin. Proc. 76 (9) (2001) 906–909.

[21] K. Nho, A. Kueider-Paisley, S. Ahmad, S. MahmoudianDehkordi, M. Arnold, S. L. Risacher, G. Louie, C. Blach, R. Baillie, X. Han, G. Kastenmüller, J. Q. Trojanowski, L.M. Shaw, M.W. Weiner, P.M. Doraiswamy, C. van Duijn, A. J. Saykin, R. Kaddurah-Daouk, Association of altered liver enzymes with Alzheimer disease diagnosis, cognition, neuroimaging measures, and cerebrospinal fluid biomarkers, JAMA Netw. Open 2 (7) (2019), e197978.

[22] D.G. Kim, A. Krenz, L.E. Toussaint, K.J. Maurer, S.A. Robinson, A. Yan, L. Torres, M.S. Bynoe, Non-alcoholic fatty liver disease induces signs of Alzheimer's disease (AD) in wild-type mice and accelerates pathological signs of AD in an AD model, J. Neuroinflamm. 13 (2016) 1.

[23] M.S. Bynoe, NAFLD induces neuroinflammation and accelerates Alzheimer's disease, J. Immunol. 196 (1 Supplement) (2016), 188.4-188.4.

[24] I. Turhan, Relationship between sugar profile and D-pinitol content of pods of wild and cultivated types of carob bean (Ceratonia siliqua L.), Int. J. Food Prop. 17 (2) (2014) 363–370.

[25] D.L. Brautigan, M. Brown, S. Grindrod, G. Chinigo, A. Kruszewski, S.M. Lukasik, J.H. Bushweller, M. Horal, S. Keller, S. Tamura, D.B. Heimark, J. Price, A. N. Larner, J. Larner, Allosteric activation of protein phosphatase 2C by D-chiro-inositol-galactosamine, a putative mediator mimetic of insulin action, Biochemistry 44 (33) (2005) 11067–11073.

[26] J. Larner, J.D. Price, D. Heimark, L. Smith, G. Rule, T. Piccariello, M.C. Fonteles, C. Pontes, D. Vale, L. Huang, Isolation, structure, synthesis, and bioactivity of a novel putative insulin mediator. A galactosamine chiro-inositol pseudo-disaccharide Mn2+ chelate with insulin-like activity, J. Med. Chem. 46 (15) (2003) 3283–3291.

[27] R. Lazarenko, J. Geisler, D. Bayliss, J. Larner, C. Li, D-chiro-inositol glycan stimulates insulin secretion in pancreatic β cells, Mol. Cell Endocrinol. 387 (1–2) (2014) 1–7.

[28] J.A. SILVA, A.C.D. Silva, L.S. Figueiredo, T.R. Araujo, I.N. Freitas, E.M. Carneiro, E.S. Ribeiro, R.A. Ribeiro, D-pinitol increases insulin secretion and regulates hepatic lipid metabolism in msg-obese mice, An. da Acad. Bras. De. Ciências 92 (2020).

[29] C. Lambert, J. Cubedo, T. Padró, G. Vilahur, S. López-Bernal, M. Rocha, A. Hernández-Mijares, L. Badimon, Effects of a carob-pod-derived sweetener on glucose metabolism, Nutrients 10 (3) (2018) 271.

[30] F. Cheng, L. Han, Y. Xiao, C. Pan, Y. Li, X. Ge, Y. Zhang, S. Yan, M. Wang, d- chiro-Inositol ameliorates high fat diet-induced hepatic steatosis and insulin resistance via PKCε-PI3K/AKT pathway, J. Agric. Food Chem. 67 (21) (2019) 5957–5967.

[31] M.M. Montt-Guevara, M. Finiguerra, I. Marzi, T. Fidecicchi, A. Ferrari, A. D. Genazzani, T. Simoncini, D-chiro-inositol regulates insulin signaling in human adipocytes, Front Endocrinol. 12 (2021), 660815.

[32] C. Fan, W. Liang, M. Wei, X. Gou, S. Han, J. Bai, Effects of D-chiro-inositol on glucose metabolism in db/db mice and the associated underlying mechanisms, Front. Pharm. 11 (2020) 354.

[33] R. Roman-Ramos, J.C. Almanza-Perez, A. Fortis-Barrera, S. Angeles-Mejia, T. R. Banderas-Dorantes, A. Zamilpa-Alvarez, M. Diaz-Flores, I. Jasso, G. Blancas-Flores, J. Gomez, F.J. Alarcon-Aguilar, Antioxidant and anti-inflammatory effects of a hypoglycemic fraction from Cucurbita ficifolia Bouché in streptozotocin-induced diabetes mice, Am. J. Chin. Med. 40 (1) (2012) 97–110.

[34] H. Oakley, S.L. Cole, S. Logan, E. Maus, P. Shao, J. Craft, A. Guillozet-Bongaarts, M. Ohno, J. Disterhoft, L. Van Eldik, R. Berry, R. Vassar, Intraneuronal β-amyloid aggregates, neurodegeneration, and neuron loss in transgenic mice with five familial Alzheimer's disease mutations: potential factors in amyloid plaque formation, J. Neurosci. 26 (40) (2006) 10129–10140.

[35] H. Oakley, S.L. Cole, S. Logan, E. Maus, P. Shao, J. Craft, A. Guillozet-Bongaarts, M. Ohno, J. Disterhoft, L. Van Eldik, R. Berry, R. Vassar, Intraneuronal beta-amyloid aggregates, neurodegeneration, and neuron loss in transgenic mice with five familial Alzheimer's disease mutations: potential factors in amyloid plaque formation, J. Neurosci. Off. J. Soc. Neurosci. 26 (40) (2006) 10129–10140.

[36] M. Ohno, L. Chang, W. Tseng, H. Oakley, M. Citron, W.L. Klein, R. Vassar, J. F. Disterhoft, Temporal memory deficits in Alzheimer's mouse models: rescue by genetic deletion of BACE1, Eur. J. Neurosci. 23 (1) (2006) 251–260.

[37] R. Kimura, L. Devi, M. Ohno, Partial reduction of BACE1 improves synaptic plasticity, recent and remote memories in Alzheimer's disease transgenic mice, J. Neurochem 113 (1) (2010) 248–261.

[38] G. Paxinos, K.B. Franklin, Paxinos and Franklin's the Mouse Brain in Stereotaxic Coordinates, Academic Press, 2019.

[39] D. Medina-Vera, C. Rosell-Valle, A.J. López-Gambero, J.A. Navarro, E. N. Zambrana-Infantes, P. Rivera, L.J. Santín, J. Suarez, F. Rodríguez de Fonseca, Imbalance of endocannabinoid/lysophosphatidylinositol receptors marks the severity of Alzheimer's disease in a preclinical model: a therapeutic opportunity, Biology 9 (11) (2020).

[40] P. Rivera, M.T. Ramírez-López, A. Vargas, J. Decara, M. Vázquez, R. Arco, R. Gómez de Heras, J. Argente, F. Rodríguez de Fonseca, J.A. Chowen, J. Suárez, Perinatal free-choice of a high-calorie low-protein diet affects leptin signaling through IRS1 and AMPK dephosphorylation in the hypothalami of female rat offspring in adulthood, Acta Physiol. 226 (2) (2019), e13244.

[41] P. Rivera, S. Guerra-Cantera, A. Vargas, F. Díaz, R. García-Úbeda, R. Tovar, M. T. Ramírez-López, J. Argente, F.R. de Fonseca, J. Suárez, J.A. Chowen, Maternal hypercaloric diet affects factors involved in lipid metabolism and the endogenous cannabinoid systems in the hypothalamus of adult offspring: sex-specific response of astrocytes to palmitic acid and anandamide, Nutr. Neurosci. (2020) 1–14.

[42] J.A. Navarro, J. Decara, D. Medina-Vera, R. Tovar, J. Suarez, J. Pavón, A. Serrano, M. Vida, A. Gutierrez-Adan, C. Sanjuan, E. Baixeras, F.Rd Fonseca, D-pinitol from ceratonia siliqua is an orally active natural inositol that reduces pancreas insulin secretion and increases circulating ghrelin levels in wistar rats, Nutrients 12 (7) (2020) 2030.

[43] J. Decara, A. Serrano, F.J. Pavón, P. Rivera, R. Arco, A. Gavito, A. Vargas, J. A. Navarro, R. Tovar, A.J. Lopez-Gambero, A. Martínez, J. Suárez, F. Rodríguez de Fonseca, E. Baixeras, The adiponectin promoter activator NP-1 induces high levels of circulating TNFα and weight loss in obese (fa/fa) Zucker rats, Sci. Rep. 8 (1) (2018) 9858.

[44] P. Rivera, A. Vargas, A. Pastor, A. Boronat, A.J. López-Gambero, L. Sánchez-Marín, D. Medina-Vera, A. Serrano, F.J. Pavón, R. de la Torre, E. Agirregoitia, M. I. Lucena, F. Rodríguez de Fonseca, J. Decara, J. Suárez, Differential hepatoprotective role of the cannabinoid CB(1) and CB(2) receptors in paracetamol-induced liver injury, Br. J. Pharm. 177 (14) (2020) 3309–3326.

[45] J. Decara, S. Arrabal, D. Beiroa, P. Rivera, A. Vargas, A. Serrano, F.J. Pavón, J. Ballesteros, C. Dieguez, R. Nogueiras, F. Rodríguez de Fonseca, J. Suárez, Antiobesity efficacy of GLP-1 receptor agonist liraglutide is associated with peripheral tissue-specific modulation of lipid metabolic regulators, Biofactors 42 (6) (2016) 600–611.

[46] J. Suárez, P. Rivera, S. Arrabal, A. Crespillo, A. Serrano, E. Baixeras, F.J. Pavón, M. Cifuentes, R. Nogueiras, J. Ballesteros, C. Dieguez, F. Rodríguez de Fonseca, Oleoylethanolamide enhances β-adrenergic-mediated thermogenesis and white-to-brown adipocyte phenotype in epididymal white adipose tissue in rat, Disease Models &amp, Mechanisms 7 (1) (2014) 129–141.

[47] R.N. Hughes, The value of spontaneous alternation behavior (SAB) as a test of retention in pharmacological investigations of memory, Neurosci. Biobehav Rev. 28 (5) (2004) 497–505.

[48] C. Rosell-Valle, C. Pedraza, I. Manuel, M. Moreno-Rodríguez, R. Rodríguez-Puertas, E. Castilla-Ortega, J.M. Caramés, A.I. Gómez Conde, E. Zambrana-Infantes, J. Ortega-Pinazo, P.J. Serrano-Castro, J. Chun, F. Rodríguez De Fonseca, L.J. Santín, G. Estivill-Torrús, Chronic central modulation of LPA/LPA receptors-signaling pathway in the mouse brain regulates cognition, emotion, and hippocampal neurogenesis, Prog. Neuropsychopharmacol. Biol. Psychiatry 108 (2021), 110156.

[49] R.G. Morris, P. Garrud, J.N. Rawlins, J. O'Keefe, Place navigation impaired in rats with hippocampal lesions, Nature 297 (5868) (1982) 681–683.
[50] A. Garthe, J. Behr, G. Kempermann, Adult-generated hippocampal neurons allow the flexible use of spatially precise learning strategies, PLoS One 4 (5) (2009), e5464.
[51] W.H. Gendron, E. Fertan, S. Pelletier, K.M. Roddick, T.P. O'Leary, Y. Anini, R. E. Brown, Age related weight loss in female 5xFAD mice from 3 to 12 months of age, Behav. Brain Res. 406 (2021), 113214.
[52] C.V. Vorhees, M.T. Williams, Morris water maze: procedures for assessing spatial and related forms of learning and memory, Nat. Protoc. 1 (2) (2006) 848–858.
[53] A.R. Meloni, M.B. DeYoung, C. Lowe, D.G. Parkes, GLP-1 receptor activated insulin secretion from pancreatic β-cells: mechanism and glucose dependence, Diabetes, Obes. Metab. 15 (1) (2013) 15–27.
[54] K. Do, B.T. Laing, T. Landry, W. Bunner, N. Mersaud, T. Matsubara, P. Li, Y. Yuan, Q. Lu, H. Huang, The effects of exercise on hypothalamic neurodegeneration of Alzheimer's disease mouse model, PLoS One 13 (1) (2018), e0190205.
[55] L.S. Robison, O.J. Gannon, M.A. Thomas, A.E. Salinero, C. Abi-Ghanem, Y. Poitelon, S. Belin, K.L. Zuloaga, Role of sex and high-fat diet in metabolic and hypothalamic disturbances in the 3xTg-AD mouse model of Alzheimer's disease, J. Neuroinflamm. 17 (1) (2020) 1–20.
[56] L. Chaskiel, A.D. Bristow, R.-M. Bluthé, R. Dantzer, A. Blomqvist, J.P. Konsman, Interleukin-1 reduces food intake and body weight in rat by acting in the arcuate hypothalamus, Brain Behav., Immun. 81 (2019) 560–573.
[57] A.P. Arruda, M. Milanski, A. Coope, A.S. Torsoni, E. Ropelle, D.P. Carvalho, J. B. Carvalheira, L.A. Velloso, Low-grade hypothalamic inflammation leads to defective thermogenesis, insulin resistance, and impaired insulin secretion, Endocrinology 152 (4) (2011) 1314–1326.
[58] N. Uyama, A. Geerts, H. Reynaert, Neural connections between the hypothalamus and the liver, Anat. Rec. A Disco Mol. Cell Evol. Biol. 280 (1) (2004) 808–820.
[59] L. Rui, Energy metabolism in the liver, Compr. Physiol. 4 (1) (2014) 177–197.
[60] S.A. Polyzos, N. Perakakis, C.S. Mantzoros, Fatty liver in lipodystrophy: A review with a focus on therapeutic perspectives of adiponectin and/or leptin replacement, Metabolism 96 (2019) 66–82.
[61] S. Müller, O. Preische, H.R. Sohrabi, S. Gräber, M. Jucker, J. Dietzsch, J. M. Ringman, R.N. Martins, E. McDade, P.R. Schofield, B. Ghetti, M. Rossor, N. R. Graff-Radford, J. Levin, D. Galasko, K.A. Quaid, S. Salloway, C. Xiong, T. Benzinger, V. Buckles, C.L. Masters, R. Sperling, R.J. Bateman, J.C. Morris, C. Laske, Decreased body mass index in the preclinical stage of autosomal dominant Alzheimer's disease, Sci. Rep. 7 (1) (2017) 1225.
[62] J. Ma, W. Zhang, H.F. Wang, Z.X. Wang, T. Jiang, M.S. Tan, J.T. Yu, L. Tan, Peripheral blood adipokines and insulin levels in patients with Alzheimer's disease: a replication study and meta-analysis, Curr. Alzheimer Res. 13 (3) (2016) 223–233.
[63] D. Kellar, S.N. Lockhart, P. Aisen, R. Raman, R.A. Rissman, J. Brewer, S. Craft, Intranasal insulin reduces white matter hyperintensity progression in association with improvements in cognition and CSF biomarker profiles in mild cognitive impairment and Alzheimer's disease, J. Prev. Alzheimers Dis. 8 (3) (2021) 240–248.
[64] S. Craft, R. Raman, T.W. Chow, M.S. Rafii, C.K. Sun, R.A. Rissman, M.C. Donohue, J.B. Brewer, C. Jenkins, K. Harless, D. Gessert, P.S. Aisen, Safety, efficacy, and feasibility of intranasal insulin for the treatment of mild cognitive impairment and Alzheimer Disease dementia: a randomized clinical trial, JAMA Neurol. 77 (9) (2020) 1099–1109.
[65] J.A. Luchsinger, T. Perez, H. Chang, P. Mehta, J. Steffener, G. Pradabhan, M. Ichise, J. Manly, D.P. Devanand, E. Bagiella, Metformin in amnestic mild cognitive impairment: results of a pilot randomized placebo controlled clinical trial, J. Alzheimers Dis. 51 (2) (2016) 501–514.
[66] G.M. Pasinetti, Compositions and methods for treating Alzheimer's disease and related disorders and promoting a healthy nervous system, Google Patents, 2014.
[67] A.M. Reilly, A.P. Tsai, P.B. Lin, A.C. Ericsson, A.L. Oblak, H. Ren, Metabolic defects caused by high-fat diet modify disease risk through inflammatory and amyloidogenic pathways in a mouse model of Alzheimer's disease, Nutrients 12 (10) (2020) 2977.
[68] A.L. Oblak, P.B. Lin, K.P. Kotredes, R.S. Pandey, D. Garceau, H.M. Williams, A. Uyar, R. O'Rourke, S. O'Rourke, C. Ingraham, D. Bednarczyk, M. Belanger, Z. A. Cope, G.J. Little, S.-P.G. Williams, C. Ash, A. Bleckert, T. Ragan, B.A. Logsdon, L.M. Mangravite, S.J. Sukoff Rizzo, P.R. Territo, G.W. Carter, G.R. Howell, M. Sasner, B.T. Lamb, Comprehensive evaluation of the 5XFAD mouse model for preclinical testing applications: a MODEL-AD study, Front. Aging Neurosci. 13 (2021).
[69] T.P. O'Leary, H.M. Mantolino, K.R. Stover, R.E. Brown, Age-related deterioration of motor function in male and female 5xFAD mice from 3 to 16 months of age, Genes, Brain Behav. 19 (3) (2020), e12538.
[70] H. White, C. Pieper, K. Schmader, The association of weight change in Alzheimer's disease with severity of disease and mortality: a longitudinal analysis, J. Am. Geriatr. Soc. 46 (10) (1998) 1223–1227.
[71] S. Gillette Guyonnet, G. Abellan Van Kan, E. Alix, S. Andrieu, J. Belmin, G. Berrut, M. Bonnefoy, P. Brocker, T. Constans, M. Ferry, A. Ghisolfi-Marque, L. Girard, R. Gonthier, O. Guerin, M.P. Hervy, P. Jouanny, M.C. Laurain, L. Lechowski, F. Nourhashemi, A. Raynaud-Simon, P. Ritz, J. Roche, Y. Rolland, T. Salva, B. Vellas, IANA (international academy on nutrition and aging) expert group: weight loss and Alzheimer's disease, J. Nutr. Health Aging 11 (1) (2007) 38–48.
[72] M.E. Soto, M. Secher, S. Gillette-Guyonnet, G. Abellan van Kan, S. Andrieu, F. Nourhashemi, Y. Rolland, B. Vellas, Weight loss and rapid cognitive decline in community-dwelling patients with Alzheimer's disease, J. Alzheimer'S. Dis. JAD 28 (3) (2012) 647–654.
[73] S. Müller, O. Preische, H.R. Sohrabi, S. Gräber, M. Jucker, J. Dietzsch, J. M. Ringman, R.N. Martins, E. McDade, P.R. Schofield, B. Ghetti, M. Rossor, N. R. Graff-Radford, J. Levin, D. Galasko, K.A. Quaid, S. Salloway, C. Xiong, T. Benzinger, V. Buckles, C.L. Masters, R. Sperling, R.J. Bateman, J.C. Morris, C. Laske, Decreased body mass index in the preclinical stage of autosomal dominant Alzheimer's disease, Sci. Rep. 7 (1) (2017) 1225.
[74] S. Jawhar, A. Trawicka, C. Jenneckens, T.A. Bayer, O. Wirths, Motor deficits, neuron loss, and reduced anxiety coinciding with axonal degeneration and intraneuronal Aβ aggregation in the 5XFAD mouse model of Alzheimer's disease, Neurobiol. Aging 33 (1) (2012) 196.e29–196.e40.
[75] A.L. Oblak, P.B. Lin, K.P. Kotredes, R.S. Pandey, D. Garceau, H.M. Williams, A. Uyar, R. O'Rourke, S. O'Rourke, C. Ingraham, D. Bednarczyk, M. Belanger, Z. A. Cope, G.J. Little, S.G. Williams, C. Ash, A. Bleckert, T. Ragan, B.A. Logsdon, L. M. Mangravite, S.J. Sukoff Rizzo, P.R. Territo, G.W. Carter, G.R. Howell, M. Sasner, B.T. Lamb, Comprehensive evaluation of the 5XFAD mouse model for preclinical testing applications: a MODEL-AD study, Front. Aging Neurosci. 13 (2021), 713726.
[76] L.S. Robison, O.J. Gannon, M.A. Thomas, A.E. Salinero, C. Abi-Ghanem, Y. Poitelon, S. Belin, K.L. Zuloaga, Role of sex and high-fat diet in metabolic and hypothalamic disturbances in the 3xTg-AD mouse model of Alzheimer's disease, J. Neuroinflamm. 17 (1) (2020) 285.
[77] A. Joly-Amado, K.S. Serraneau, M. Brownlow, C. Marín de Evsikova, J. R. Speakman, M.N. Gordon, D. Morgan, Metabolic changes over the course of aging in a mouse model of tau deposition, Neurobiol. Aging 44 (2016) 62–73.
[78] W.H. Gendron, E. Fertan, S. Pelletier, K.M. Roddick, T.P. O'Leary, Y. Anini, R. E. Brown, Age related weight loss in female 5xFAD mice from 3 to 12 Months of Age, Behav. Brain Res. (2021), 113214.
[79] M. Maulik, D. Westaway, J.H. Jhamandas, S. Kar, Role of cholesterol in APP metabolism and its significance in Alzheimer's disease pathogenesis, Mol. Neurobiol. 47 (1) (2013) 37–63.
[80] R. Williamson, C. Sutherland, Neuronal membranes are key to the pathogenesis of Alzheimer's disease: the role of both raft and non-raft membrane domains, Curr. Alzheimer Res 8 (2) (2011) 213–221.
[81] F.F. de Oliveira, E.S. Chen, M.C. Smith, P.H.F. Bertolucci, Longitudinal lipid profile variations and clinical change in Alzheimer's disease dementia, Neurosci. Lett. 646 (2017) 36–42.
[82] I. Kaya, E. Jennische, J. Dunevall, S. Lange, A.G. Ewing, P. Malmberg, A. T. Baykal, J.S. Fletcher, Spatial lipidomics reveals region and long chain base specific accumulations of monosialogangliosides in amyloid plaques in familial Alzheimer's disease mice (5xFAD) brain, ACS Chem. Neurosci. 11 (1) (2020) 14–24.
[83] J.H. Hong, J.W. Kang, D.K. Kim, S.H. Baik, K.H. Kim, S.R. Shanta, J.H. Jung, I. Mook-Jung, K.P. Kim, Global changes of phospholipids identified by MALDI imaging mass spectrometry in a mouse model of Alzheimer's disease, J. Lipid Res. 57 (1) (2016) 36–45.
[84] R. Tabrizi, V. Ostadmohammadi, K.B. Lankarani, P. Peymani, M. Akbari, F. Kolahdooz, Z. Asemi, The effects of inositol supplementation on lipid profiles among patients with metabolic diseases: a systematic review and meta-analysis of randomized controlled trials, Lipids Health Dis. 17 (1) (2018) 123.
[85] R. Peila, B.L. Rodriguez, L.R. White, L.J. Launer, Fasting insulin and incident dementia in an elderly population of Japanese-American men, Neurology 63 (2) (2004) 228–233.
[87] M. Vandal, P.J. White, G. Chevrier, C. Tremblay, I. St.-Amour, E. Planel, A. Marette, F. Calon, Age-dependent impairment of glucose tolerance in the 3xTg-AD mouse model of Alzheimer's disease, FASEB J. 29 (10) (2015) 4273–4284.
[88] S. Sivakumar, S.P. Subramanian, Pancreatic tissue protective nature of D-Pinitol studied in streptozotocin-mediated oxidative stress in experimental diabetic rats, Eur. J. Pharm. 622 (1–3) (2009) 65–70.
[89] Y. Yao, F. Shan, J. Bian, F. Chen, M. Wang, G. Ren, D-chiro-inositol-enriched tartary buckwheat bran extract lowers the blood glucose level in KK-Ay mice, J. Agric. Food Chem. 56 (21) (2008) 10027–10031.
[90] J.A.D. Silva JÚnior, A. Silva, L.S. Figueiredo, T.R. Araujo, I.N. Freitas, E. M. Carneiro, E.S. Ribeiro, R.A. Ribeiro, D-pinitol increases insulin secretion and regulates hepatic lipid metabolism in msg-obese mice, Acad. Bras. Cienc. 92 (4) (2020), e20201382.
[91] C. Brandscheid, F. Schuck, S. Reinhardt, K.H. Schäfer, C.U. Pietrzik, M. Grimm, T. Hartmann, A. Schwiertz, K. Endres, Altered gut microbiome composition and tryptic activity of the 5xFAD Alzheimer's mouse model, J. Alzheimers Dis. 56 (2) (2017) 775–788.
[92] M.M. Rodríguez-Peña, B. Astiarraga, J. Seco, V. Ceperuelo-Mallafré, A. Caballé, V. Pérez-Brocal, C.S. Attolini, A. Moya, G. Llauradó, A. Megía, S. Pellitero, N. Vilarrasa, S. Fernández-Veledo, J. Vendrell, Changes in glucagon-like peptide 1 and 2 levels in people with obesity after a diet-induced weight-loss intervention are related to a specific microbiota signature: a prospective cohort study, Clin. Transl. Med. 11 (11) (2021), e575.
[93] C. Zhang, W. Wu, X. Xin, X. Li, D. Liu, Extract of ice plant (Mesembryanthemum crystallinum) ameliorates hyperglycemia and modulates the gut microbiota composition in type 2 diabetic Goto-Kakizaki rats, Food Funct. 10 (6) (2019) 3252–3261.
[94] C.H. de Koning, C. Popp-Snijders, J. Schoemaker, C.B. Lambalk, Elevated FSH concentrations in imminent ovarian failure are associated with higher FSH and LH pulse amplitude and response to GnRH, Hum. Reprod. 15 (7) (2000) 1452–1456.
[95] E.R. Bertone-Johnson, J.K. Virtanen, L. Niskanen, T. Nurmi, K. Ronkainen, S. Voutilainen, J. Mursu, J. Kauhanen, T.-P. Tuomainen, Association of follicle-

stimulating hormone levels and risk of type 2 diabetes in older postmenopausal women, Menopause 24 (7) (2017) 796–802.
[96] M. Balietti, C. Giuli, P. Fattoretti, P. Fabbietti, R. Papa, D. Postacchini, F. Conti, Effect of a comprehensive intervention on plasma BDNF in patients with Alzheimer'S Disease, J. Alzheimer'S. Dis. JAD 57 (1) (2017) 37–43.
[97] G. Allan, C. Mobbs, Use of D-chiro-inositol in the treatment of conditions associated with hypothalamic gene expression, Google Patents, 2002.
[98] A. Seth, S. Stanley, W. Dhillo, K. Murphy, M. Ghatei, S. Bloom, Effects of galanin-like peptide on food intake and the hypothalamo-pituitary-thyroid axis, Neuroendocrinology 77 (2) (2003) 125–131.
[99] N.S. Singhal, M.A. Lazar, R.S. Ahima, Central resistin induces hepatic insulin resistance via neuropeptide Y, J. Neurosci. 27 (47) (2007) 12924–12932.
[100] L. Chaskiel, A.D. Bristow, R.M. Bluthé, R. Dantzer, A. Blomqvist, J.P. Konsman, Interleukin-1 reduces food intake and body weight in rat by acting in the arcuate hypothalamus, Brain Behav. Immun. 81 (2019) 560–573.
[101] F.M. Chaves, N.S. Mansano, R. Frazão, J. Donato, Tumor necrosis factor α and interleukin-1β acutely inhibit AgRP neurons in the arcuate nucleus of the hypothalamus, Int. J. Mol. Sci. 21 (23) (2020) 8928.
[102] A.P. Arruda, M. Milanski, A. Coope, A.S. Torsoni, E. Ropelle, D.P. Carvalho, J. B. Carvalheira, L.A. Velloso, Low-grade hypothalamic inflammation leads to defective thermogenesis, insulin resistance, and impaired insulin secretion, Endocrinology 152 (4) (2011) 1314–1326.
[103] V.C. Bobbo, D.F. Engel, C.P. Jara, N.F. Mendes, R. Haddad-Tovolli, T.P. Prado, D. Sidarta-Oliveira, J. Morari, L.A. Velloso, E.P. Araujo, Interleukin-6 actions in the hypothalamus protects against obesity and is involved in the regulation of neurogenesis, J. Neuroinflamm. 18 (1) (2021) 192.
[104] S.-E. Park, R. Dantzer, K.W. Kelley, R.H. McCusker, Central administration of insulin-like growth factor-I decreases depressive-like behavior and brain cytokine expression in mice, J. Neuroinflamm. 8 (1) (2011) 12.
[105] J.L. Labandeira-Garcia, M.A. Costa-Besada, C.M. Labandeira, B. Villar-Cheda, A. I. Rodríguez-Perez, Insulin-like growth factor-1 and neuroinflammation, Front. Aging Neurosci. 9 (2017).
[106] F. Cheng, S.-j Yun, J.-l Cao, M.-c Chang, J.-l Meng, J.-y Liu, Y.-f Cheng, C.-p Feng, Differential gene expression and biological analyses of primary hepatocytes following D-chiro-inositol supplement, Front. Endocrinol. 12 (2021).
[107] S.-s Zhao, N.-r Li, W.-l Zhao, H. Liu, M.-x Ge, Y.-x Zhang, L.-y Zhao, X.-f You, H.-w He, R.-g Shao, D-chiro-inositol effectively attenuates cholestasis in bile duct ligated rats by improving bile acid secretion and attenuating oxidative stress, Acta Pharmacol. Sin. 39 (2) (2018) 213–221.
[108] B. Xia, G.H. Cai, H. Yang, S.P. Wang, G.A. Mitchell, J.W. Wu, Adipose tissue deficiency of hormone-sensitive lipase causes fatty liver in mice, PLoS Genet. 13 (12) (2017), e1007110.
[109] X.-M. Liu, H.C. Chan, G.-L. Ding, J. Cai, Y. Song, T.-T. Wang, D. Zhang, H. Chen, M.K. Yu, Y.-T. Wu, F. Qu, Y. Liu, Y.-C. Lu, E.Y. Adashi, J.-Z. Sheng, H.-F. Huang, FSH regulates fat accumulation and redistribution in aging through the Gαi/Ca2+/CREB pathway, Aging Cell 14 (3) (2015) 409–420.
[110] H. Cui, G. Zhao, R. Liu, M. Zheng, J. Chen, J. Wen, FSH stimulates lipid biosynthesis in chicken adipose tissue by upregulating the expression of its receptor FSHR, J. Lipid Res. 53 (5) (2012) 909–917.
[111] Y. Zhu, J. Xu, X. Zhang, Y. Ke, G. Fu, Q. Guo, A low follicle-stimulating hormone level is a protective factor for non-alcoholic fatty liver disease in older men aged over 80, BMC Geriatr. 21 (1) (2021) 544.
[112] J. Manna, G.L. Dunbar, P. Maiti, Curcugreen treatment prevented splenomegaly and other peripheral organ abnormalities in 3xTg and 5xFAD mouse models of Alzheimer's disease, Antioxidants 10 (6) (2021) 899.
[113] V. Lam, R. Takechi, M.J. Hackett, R. Francis, M. Bynevelt, L.M. Celliers, M. Nesbit, S. Mamsa, F. Arfuso, S. Das, F. Koentgen, M. Hagan, L. Codd, K. Richardson, B. O'Mara, R.K. Scharli, L. Morandeau, J. Gauntlett, C. Leatherday, J. Boucek, J.C. L. Mamo, Synthesis of human amyloid restricted to liver results in an Alzheimer disease-like neurodegenerative phenotype, PLoS Biol. 19 (9) (2021), e3001358.
[114] S. Softic, M. Kirby, N.G. Berger, N.F. Shroyer, S.C. Woods, R. Kohli, Insulin concentration modulates hepatic lipid accumulation in mice in part via transcriptional regulation of fatty acid transport proteins, PLoS One 7 (6) (2012), e38952.
[115] J.N. Kim, S.N. Han, H.K. Kim, Phytic acid and myo-inositol support adipocyte differentiation and improve insulin sensitivity in 3T3-L1 cells, Nutr. Res. 34 (8) (2014) 723–731.